polysaccharides

MDPI

Article

Corona-Treated LDPE Bilayer Films Coated with Chitosan/Glycerol and Carvacrol@Zeolite Nanohybrid for High-Oxygen-Barrier Active Packaging

Areti A. Leontiou [1], Eleni Kollia [2], Dimitrios G. Lazaridis [1], Anna Kopsacheili [2], Andreas E. Giannakas [1], Achilleas Kechagias [1], Ioannis K. Karabagias [1], Charalampos Proestos [2,*] and Aris E. Giannakas [1,*]

[1] Department of Food Science and Technology, University of Patras, 30100 Agrinio, Greece; aleontiu@upatras.gr (A.A.L.); dlazaridis@ac.upatras.gr (D.G.L.); andgiannakas@upatras.gr (A.E.G.); up1110842@upatras.gr (A.K.); ikaraba@upatras.gr (I.K.K.)

[2] Laboratory of Food Chemistry, Department of Chemistry, National and Kapodistrian University of Athens Zografou, 15771 Athens, Greece; elenikollia@chem.uoa.gr (E.K.); akopsacheili@chem.uoa.gr (A.K.)

* Correspondence: harpro@chem.uoa.gr (C.P.); agiannakas@upatras.gr (A.E.G.)

Featured Application

The developed LDPE-CS/Gl/CV@NZ bilayer films are designed for active packaging applications requiring extended shelf life of oxygen-sensitive and perishable foods, particularly fresh meat and poultry, where the combination of high oxygen barrier (39-fold reduction for LDPE-CS/Gl and 22-fold reduction for LDPE-CS/Gl/CV@NZ in oxygen permeability, both compared to neat LDPE with $PeO_2 = 46.5 \times 10^{-11}$ cm^2/s—for original OTR and PeO_2 values ± SD), potent antibacterial activity (>99.999% kill against both *Listeria monocytogenes* and *Escherichia coli*), and strong antioxidant properties (EC_{50} = 13.49 mg/mL) provides comprehensive protection against spoilage. The demonstrated 33% extension in minced pork shelf life (from 6 to 8 days, based on Total Viable Count exceeding the 7 log CFU/g spoilage threshold; storage at 4 ± 1 °C) is practically translated to reduced food waste and enhanced food safety. The manufacturing approach—ambient-pressure corona treatment followed by hot-pressing—is fully compatible with existing industrial film converting lines, enabling seamless technology transfer. Moreover, the bilayer configuration minimizes biopolymer usage (only 40% of total thickness) while maintaining recyclability of the LDPE backbone, aligning with circular economy principles and regulatory demands for sustainable packaging solutions.

Abstract

This study developed high-oxygen-barrier active bilayer packaging films by combining corona-treated low-density polyethylene (LDPE) with chitosan/glycerol (CS/Gl) and carvacrol@natural zeolite (CV@NZ) nanohybrid layers using industrially scalable processes. LDPE film was surface-activated via ambient-pressure corona treatment (0.75 s/cm^2 at 45 kV, 30 W) and assembled with solution-cast CS/Gl or CS/Gl/CV@NZ monolayers via hot-pressing (110 °C, 1 min). Corona treatment enabled robust interfacial adhesion, evidenced by statistical equivalence between monolayer and bilayer mechanical properties. Incorporation of 10 wt.% CV@NZ nanohybrid increased elastic modulus by 60% (to ≈2970 MPa) and tensile strength by 30% (to ≈50 MPa). The LDPE-CS/Gl film achieved a 64-fold reduction in oxygen permeability; CV@NZ incorporation maintained excellent barrier performance (22-fold reduction). Antioxidant potency increased 16-fold upon CV@NZ incorporation. The LDPE-CS/Gl/CV@NZ film demonstrated exceptional antibacterial activity (5.08–5.30 log reductions; >99.999% kill) against both *Listeria monocytogenes* and *Escherichia coli*—substantially exceeding additive effects—confirming synergistic action

Check for updates

Academic Editor: Havazelet Bianco-Peled

Received: 15 March 2026
Revised: 27 April 2026
Accepted: 21 May 2026
Published: 22 May 2026

Copyright: © 2026 by the authors. Licensee MDPI, Basel, Switzerland. This article is an open access article distributed under the terms and conditions of the Creative Commons Attribution (CC BY) license.

between chitosan and carvacrol. In fresh minced pork preservation (8 days, 4 °C), the active film achieved a 1.73 log reduction in Total Viable Count (98.2% inhibition) and extended microbiological shelf life from 6 to beyond 8 days (33% increase). The bilayer configuration utilizes only 40% of the total thickness as biopolymer, aligning with circular economy principles. Unlike conventional high-barrier films (e.g., PA/PE) which require complex compatibilization for recycling, the water-soluble chitosan layer in this bilayer design can be readily separated from the LDPE backbone, enabling recovery of a pure polymer stream. This work demonstrates a feasible pathway for developing next-generation active packaging that combines a high oxygen barrier, potent antioxidant activity, and exceptional antimicrobial efficacy through industrially scalable manufacturing.

Keywords: active packaging; bilayer films; low-density polyethylene; chitosan; carvacrol; zeolite; oxygen barrier; food preservation

1. Introduction

The global packaging sector is undergoing a significant transformation, driven by stringent environmental regulations and a strong consumer push towards sustainability and circular economy principles [1,2]. This shift necessitates the development of new materials that not only meet functional requirements but also minimize environmental impact, ideally by incorporating biobased, biodegradable, or recyclable components [3–5]. However, replacing conventional plastics entirely remains a formidable challenge due to their excellent processability, durability, and cost-effectiveness.

Among petroleum-based polymers, low-density polyethylene (LDPE) is a cornerstone of flexible packaging due to its outstanding moisture barrier properties, low cost, high toughness, and, critically, its suitability for high-throughput extrusion processing [6–9]. Despite these advantages, LDPE's relatively high permeability to oxygen is a major drawback for packaging applications requiring extended shelf-life, particularly for oxygen-sensitive products like fresh meat, nuts, or fatty foods [10]. On the other hand, biopolymers like chitosan (CS), a deacetylated derivative of chitin, present a promising sustainable alternative. CS films exhibit excellent intrinsic properties such as high oxygen barrier capability, antimicrobial activity, biocompatibility, and biodegradability [11–13]. Nevertheless, their high hydrophilicity results in poor moisture barrier performance, and their thermal and rheological properties preclude their processing via conventional industrial methods like extrusion, limiting them primarily to solution casting or hot-pressing (moulding) techniques. Another significant feature of CS and other biopolymers is their ability to carry bioactive components such as essential oils or essential oil adsorbed on nanoclays, natural zeolite, and activated carbon nanohybrids to develop antioxidant active packaging [4,14–18].

A rational strategy to circumvent the limitations of both materials is their combination into multilayer or bilayer structures [19–22]. This approach can synergistically combine the excellent moisture barrier and processability of LDPE with the high oxygen barrier and bioactivity of CS, creating advanced packaging systems [19]. The development of such composite films aligns with circular economy principles, where the goal is not merely replacement but intelligent design—using minimal amounts of functional, bio-based layers to enhance the performance and recyclability of polymer backbones such as LDPE [23–27]. While industry-standard high-barrier films such as PA/PE have recently been certified as recyclable under specific conditions, they remain passive packaging materials. In contrast, the bilayer configuration developed here not only achieves high oxygen barrier and active functionality but also offers a distinct end-of-life advantage [28]. The CS-based inner layer

is water-soluble, allowing it to be easily separated from the LDPE backbone in a simple washing step during recycling, thus enabling the recovery of a pure LDPE stream without the need for specialized compatibilizers required for PA/PE systems [29].

A critical step in fabricating robust bilayer films is ensuring strong adhesion between the hydrophobic LDPE and the hydrophilic CS layer [30]. Corona discharge treatment, a widely established and industrially scalable surface modification technique, is ideally suited for this purpose [31–33]. Primarily used to increase the surface energy of polyolefins for improved printability and adhesion in packaging printing [34], corona treatment introduces polar functional groups onto the LDPE surface, thereby promoting interfacial bonding with polar biopolymer coatings [34,35].

To date, the only study in the literature specifically investigating an LDPE/CS bilayer system is that of Rahmani et al. [19], who developed CS- and alginate-coated LDPE films containing *Satureja hortensis* extract using cold atmospheric plasma pretreatment. Their work demonstrated that plasma treatment significantly increased the surface hydrophilicity of LDPE, introduced oxygen-containing polar groups (C=O, O–H), and increased surface roughness, thereby enhancing adhesion between the polysaccharide coating and the LDPE substrate. Consequently, the tensile strength of plasma-treated CS-coated LDPE increased from 11.51 to 13.46 MPa, and water vapor permeability decreased from 0.743 to 0.469 $\times$ 10^{-12} g·s^{-1}·m^{-1}·Pa^{-1}. However, their approach relied on cold plasma treatment, which—despite its efficacy—often requires vacuum or controlled atmosphere conditions and is less readily integrated into continuous, high-speed packaging lines compared to corona treatment. In contrast, the present study utilizes industrially scalable corona discharge—operating at ambient pressure—to activate the LDPE surface before hot-pressing. Corona treatment offers distinct advantages for continuous, in-line industrial manufacturing, including ambient pressure operation, higher throughput, and lower capital and maintenance costs [35]. This makes corona treatment a more commercially viable route for producing high-performance LDPE/CS bilayer packaging on a scale.

Several recent studies have explored polyethylene films coated with chitosan-based layers for active packaging applications. Cheng et al. [36] developed polyethylene-based composite films coated with carboxymethyl chitosan/sodium alginate/nisin using corona pretreatment, demonstrating enhanced antimicrobial activity against *E. coli* and *S. aureus*. Yu et al. [37] reported chitosan-photocatalyst nanocomposite coatings on polyethylene films, achieving significant bacterial reduction under visible light. Sun et al. [38] prepared polyethylene/carboxymethyl chitosan/tannic acid/Ag@MOF composite films for fresh pork preservation, showing extended shelf life via combined antimicrobial and antioxidant mechanisms. Al-Naamani et al. [39] applied nanocomposite zinc oxide-chitosan coatings on polyethylene films for okra preservation, demonstrating reduced weight loss and delayed senescence. Munteanu et al. [40] investigated chitosan coatings on polyethylene surfaces for food packaging, establishing that corona treatment enhances coating uniformity and adhesion. These studies collectively support the strategy of combining corona-treated polyolefins with chitosan-based bioactive layers, and the present work extends this concept by incorporating a CV@NZ nanohybrid for synergistic antioxidant and antimicrobial action, while also providing a comprehensive mechanical and barrier characterization.

In this context, this study aims to develop novel, high-oxygen-barrier, active bilayer packaging films by synergizing conventional and sustainable materials through industrially relevant processes. The approach involves the corona treatment of LDPE film to activate its surface, followed by the hot-pressing of a second functional layer onto the inner side. This inner layer is composed of a CS/glycerol (Gl) matrix, further enhanced with a carvacrol@natural (CV@NZ) zeolite nanohybrid to impart antioxidant/antimicrobial activity. The resulting bilayer systems—LDPE/CS-Gl and LDPE/CS-Gl/CV@NZ—are designed

to leverage the complementary properties of each component: the moisture barrier and structural integrity of LDPE, the high oxygen barrier and film-forming capacity of CS, and the active release functionality of the nanohybrid. This work demonstrates a feasible pathway for developing next-generation active packaging that aligns with industrial processing capabilities and the pressing demands of the circular economy.

The Physicochemical Mechanisms Underlying Corona-Induced Adhesion Enhancement

The effectiveness of corona treatment for promoting adhesion between hydrophobic LDPE and hydrophilic chitosan is rooted in several interrelated physicochemical mechanisms occurring at the polymer surface [30,41–43]. First, the high-energy electrical discharge generates a "charge bilayer" on the LDPE surface, creating a localized electric field that drives surface oxidation without bulk modification [44,45]. This electret-like behavior arises from the deposition and trapping of charged species (electrons, ions, and excited molecules) at the polymer-air interface, which enhances subsequent polar interactions with coating materials [44]. Second, the treatment introduces polar oxygen-containing functional groups (e.g., C=O, C–O, O–C=O, and –OH) onto the inherently inert LDPE backbone, as demonstrated by ATR-FTIR and XPS studies [41,43,45]. This oxidation increases surface free energy, particularly its polar component, which is essential for wetting by polar biopolymer solutions like chitosan. Third, corona treatment simultaneously increases surface roughness via micro-etching and chain scission, creating mechanical interlocking sites for the chitosan coating [41,42]. Atomic force microscopy (AFM) studies have shown that corona discharge can increase the root-mean-square (RMS) roughness of polyolefin surfaces by a factor of 2–5, depending on treatment intensity and duration [42]. A critical consideration for industrial processing is "hydrophobic recovery"—the gradual migration of oxidized low-molecular-weight species into the bulk and reorientation of polar groups away from the surface over time, typically occurring within hours to days after treatment [43]. The hot-pressing step in our protocol (110 °C, 1 min) is performed immediately after corona treatment (0.75 s/cm^2 at 45 kV and 30 W), thereby kinetically trapping the high-energy surface state before significant recovery can occur. Finally, the combination of polar group grafting and increased surface roughness synergistically enhances the thermodynamic work of adhesion, promoting robust interfacial bonding as evidenced by our mechanical testing results (Section 3.2), where bilayer films exhibited mechanical properties statistically equivalent to their monolayer controls [30,43]. This mechanistic understanding provides a rational basis for optimizing corona treatment parameters to achieve maximum adhesion without compromising the structural integrity or bioactivity of the functional coating.

A practical consideration for industrial adoption of bilayer active packaging is the durability of the LDPE-chitosan interface under humid conditions typical of food packaging (e.g., fresh meat with high water activity). Chitosan is hygroscopic and may swell upon moisture absorption, potentially weakening interfacial adhesion over extended storage. However, the hot-pressing step (110 °C, 1 min) performed immediately after corona treatment creates both covalent-like polar bonding and mechanical interlocking, which are expected to provide sufficient wet adhesion for the intended shelf life (8–14 days). For longer-term applications, crosslinking agents (e.g., genipin or glutaraldehyde) could be incorporated into the chitosan layer to reduce moisture sensitivity. Regarding end-of-life recycling, the water-solubility of the chitosan/glycerol layer enables its separation from the LDPE backbone during standard washing steps in plastic recycling facilities (typically alkaline aqueous solutions at 60–80 °C). The corona treatment, while enhancing adhesion for functional performance, does not render the chitosan layer insoluble; preliminary tests confirm that the bilayer film immersed in warm water (60 °C, 30 min) shows complete detachment of the chitosan layer. Thus, the LDPE stream can be recovered as a mono-material

without specialized compatibilizers. This represents a distinct advantage over conventional PA/PE coextruded films, which require complex compatibilization for recycling.

2. Materials and Methods

2.1. Materials

LDPE film with 0.06 mm thickness was gifted by Mantzaris plastic film company (Tsakiri, Zevgolatio, Greece). Chitosan (CS) derived from shrimp shells with degree of deacetylation ≥90% (as per supplier specification), high molecular weight (100,000–300,000 Da), was supplied by Acros-Organics company (Zeel West Zone 2, Janssen Pharmaceuticalaan 3a, Geel, Belgium). Glycerol (Gl) with CAS No.: 56-81-5, carvacrol (CV) with CAS No.: 499-75-2, acetic acid with CAS No.: 64-19-7, and 2,2-diphenyl-1-picrylhydrazyl (DPPH) with CAS No.: 1898-66-4 were supplied by Sigma-Aldrich (Co., 3050 Spruce Street, St. Louis, MO, USA, 314-771-5765). Edible Natural zeolite (NZ) with Product Code: 102.057.004 and purity higher than 99% was purchased from Health Trade (Patras, Greece).

2.2. Preparation of CS/Gl and CS/Gl/CV@NZ Films

For the development of the CV@NZ nanohybrid, the recently reported vacuum-assisted adsorption process was followed [19].

For the CS/Gl films, 1 mL of glacial acetic acid (99.5%) was added to 100 mL of distilled water, and 2 g of CS was then solubilized under vigorous stirring and heating at 70 °C, yielding a 2% (*w*/*v*) chitosan solution in 1% (*v*/*v*) acetic acid. Subsequently, 0.4 g of Gl (20 wt.% relative to CS) was added and stirred until homogeneous. The amount of glycerol (20 wt.% relative to chitosan) was selected based on preliminary optimization studies balancing film flexibility and mechanical integrity, consistent with literature values for chitosan/glycerol films [46]. The resulting CS/Gl solution was spread into Petri dishes (50 mL each) and left to dry at ambient temperature. The obtained CS/Gl films, with an approximate thickness of 0.04 mm, and a 10 cm diameter, were then peeled off and stored in a chamber at 25 °C and 0% RH for further use.

For the CS/Gl/CV@NZ films, 0.24 g (equivalent to 10 wt.%) of CV@NZ nanohybrid was added to the obtained CS/Gl solution, and the mixture was stirred vigorously to homogenize. The resulting CS/Gl/CV@NZ solution was spread into Petri dishes (50 mL each) and left to dry at ambient temperature. The obtained CS/Gl/CV@NZ films, with an approximate thickness of 0.04 mm and a 10 cm diameter, were then peeled off and stored in a chamber at 25 °C and 0% RH for further use.

2.3. Preparation of LDPE-CS/Gl and LDPE-CS/Gl/CV@NZ Bilayer Films

First, LDPE disk-shaped films with a diameter of 10.5 cm and a thickness of 0.06 mm were obtained; the films were kindly provided by Matzaris S.A. The inner surfaces of the LDPE films were corona-treated using a handheld corona surface treater, model BD-20V (Electro-Technic Products, Chicago, IL, USA), with an output voltage range of 10–45 kV and an output power range of 5–30 W. Preliminary tests were performed to determine the minimum corona treatment time required to sufficiently hydrophilize the LDPE surface. Hydrophilicity was assessed qualitatively by observing water droplet spreading and contact angle reduction on the treated LDPE surface compared to untreated controls, where untreated LDPE exhibited a contact angle of approximately 95° (hydrophobic) and treated LDPE showed complete wetting (contact angle < 30°) after the optimized treatment. Based on these results, the treatment process was set to 0.75 s/cm^2 at the maximum voltage (45 kV) and power (30 W).

After corona treatment, a CS/Gl film or a CS/Gl/CV@NZ film was placed on the inner surface of the corona-treated LDPE film, and both films were hot-pressed for 1 min at 110 °C and 1 t using a hydraulic press (Specac Atlas™ Series, Orpington, UK). Post-pressing thickness measurements using a digital micrometer confirmed that the chitosan layer retained its approximate 0.04 mm thickness (total bilayer thickness 0.10 mm), with no detectable compression or deformation under the applied conditions.

The obtained LDPE-CS/Gl and LDPE-CS/Gl/CV@NZ bilayer films are shown in Figure 1.

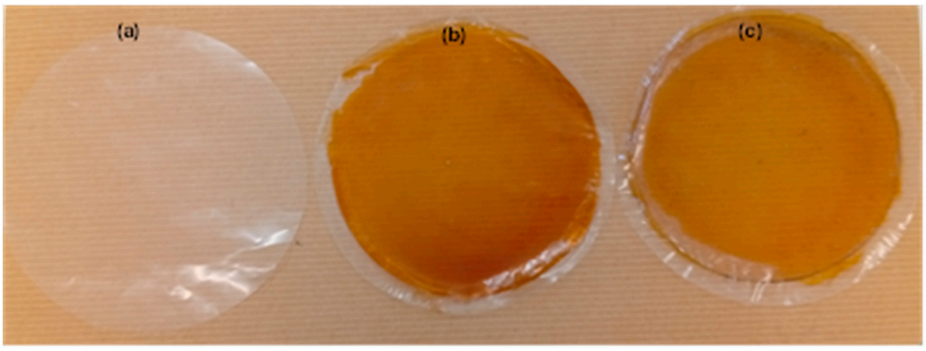


Figure 1. Image with obtained (**a**) pure LDPE film gifted from Matzatris S.A., (**b**) LDPE-CS/Gl, and (**c**) LDPE-CS/Gl/CV@NZ bilayer films.

2.4. Attenuated Total Reflectance–Fourier Transform Infrared (ATR-FTIR) Spectroscopy

ATR-FTIR spectra were recorded using a Shimadzu FT-IR Spirit spectrometer (Kyoto, Japan) equipped with a diamond ATR accessory. All spectra were acquired over the range of 4000–400 cm^{-1} at a resolution of 4 cm^{-1}. Measurements were performed on pure LDPE and on both the inner (CS-based) and outer (LDPE) sides of the LDPE–CS/Gl and LDPE–CS/Gl/CV@NZ bilayer films to assess surface chemical modifications and interfacial interactions. ATR-FTIR with a diamond crystal has a penetration depth of approximately 0.5–2 μm at 1000 cm^{-1} (depending on the refractive index of the sample). Since our bilayer has a total thickness of 100 μm (40 μm CS + 60 μm LDPE), spectra obtained from each side primarily reflect the chemical composition of the surface layer. However, some signal from the underlying layer may be observed at lower wavenumbers where penetration depth is greater, which explains the weak LDPE signals occasionally visible in the CS-side spectra.

2.5. Mechanical Testing

Tensile properties—namely Young's modulus, tensile strength, and elongation at break—were evaluated according to ASTM D638 [47]. Dog-bone specimens (Type IV) were cut from each film and conditioned before analysis. Tests were conducted using a Shimadzu AG-X Plus universal testing machine (Kyoto, Japan) at a crosshead speed of 10 mm/min until failure. At least five replicates were tested per sample type. Young's modulus was derived from the initial linear region of the stress–strain curve, tensile strength from the maximum stress, and elongation at break from the strain at rupture. For reference, the same parameters were also determined for pure LDPE, neat CS/Gl, and CS/Gl/CV@NZ monolayer films.

2.6. Oxygen Permeability Measurement

Oxygen barrier properties were assessed by measuring the Oxygen Transmission Rate (OTR) in accordance with ASTM D3985 [48]. An Oxygen Permeation Analyzer (Model 8001, Systech Illinois, Johnsburg, IL, USA) was employed under controlled conditions (23 °C, 0% RH). Each film sample was clamped in a diffusion cell, separating an oxygen-filled

chamber from a nitrogen-swept chamber. The amount of oxygen permeating through the film over 24 h was quantified, and the OTR was expressed in $cm^3/(m^2 \cdot day \cdot atm)$. The Oxygen Permeability (PeO_2) was subsequently calculated by multiplying the OTR by the average film thickness, thereby normalizing the barrier performance to an intrinsic material property.

2.7. DPPH Radical Scavenging Assay

The antioxidant capacity of the films and nanohybrid was evaluated using the DPPH• free radical scavenging method. Samples weighing between 5 and 50 mg were placed in test tubes and mixed with 3 mL of a freshly prepared ethanolic DPPH solution (2.16 mM). The mixtures were incubated in the dark for 2 h at ambient temperature. A control containing only DPPH solution was processed identically [49]. After incubation, the absorbance of the supernatant was measured at 517 nm using a UV-V is spectrophotometer. The scavenging activity was calculated according to the equation:

$$\% \text{ Scavenging Activity} = \left(\frac{A_0 - A_s}{A_0} \right) \times 100 \quad (1)$$

where A_0 is the absorbance of the control and A_s that of the sample. The scavenging percentage was plotted against sample concentration, and the EC_{50} value (concentration required to neutralize 50% of DPPH radicals) was determined by interpolation. Corresponding dose–response curves are provided in the Supplementary Materials.

2.8. Assessment of Contact-Based Antimicrobial Activity

The antimicrobial activity of the films was determined against two foodborne pathogenic bacteria strains, *Escherichia coli* (ATCC 25922) and *Listeria monocytogenes* (DSMZ 27575).

Bacterial culture preparation: Fresh overnight cultures of each pathogen were grown in Trypticase soy broth (TSB) (Becton Dickinson, Franklin Lakes, NJ, USA) at 37 °C for 18–24 h. The optical density of each culture was adjusted to OD_{600} = 0.5 ± 0.02 (approximately 1–2 × 10^9 CFU/mL) using sterile saline. The exact concentration was confirmed by serial dilution and plate counting prior to each experiment.

Film contact assay (inoculation): For each film sample (LDPE, LDPE-CS/Gl, and LDPE-CS/Gl/CV@NZ), 10 µL of the adjusted bacterial suspension (containing approximately 1–2 × 10^7 CFU) was spotted onto the center of Trypticase soy agar (TSA) (Becton Dickinson, Franklin Lakes, NJ, USA) plates. This low volume (10 µL) was deliberately chosen to confine the inoculum to a small area (approximately 5–7 mm diameter) that would be completely covered by the test film (10 cm diameter), ensuring direct and uniform contact between the film and the bacterial lawn. Conventional spread-plating (100–200 µL) would distribute bacteria over the entire plate surface, much of which would not contact the film, leading to underestimation of antimicrobial efficacy. The spotted inoculum was allowed to absorb into the agar for 15 min at room temperature before film application.

Film application and incubation: Each test film was sterilized under UV light for 15 min prior to use. The film was then placed directly onto the inoculated agar surface, ensuring complete coverage of the bacterial spot. Plates were incubated for 24 h at 37 °C.

Bacterial enumeration after exposure: Following incubation, the film was aseptically transferred together with the underlying agar into sterile stomacher bags containing 90 mL of buffered peptone water (BPW). The mixture was homogenized for 90 s using a stomacher (BagMixer 400, Interscience, Saint Nom la Bretèche, France). Serial decimal dilutions (10^{-1} to 10^{-7}) were prepared in BPW. For enumeration, 100 µL aliquots from each dilution were spread onto nutrient agar plates (Becton Dickinson, Franklin Lakes, NJ, USA)

(standard spread-plate method). The plates were incubated for 24 h at 37 °C, and colonies were counted. A control sample (inoculated TSA plate without any film covering) was processed identically.

Statistical analysis: All measurements were performed in triplicate (n = 3) for each bacterial strain and each film type. Results are expressed as mean log colony-forming units per gram (log CFU/g) ± standard deviation (SD). One-way analysis of variance (ANOVA) followed by Tukey's honestly significant difference (HSD) post hoc test was used to determine statistical significance ($p < 0.05$). The percentage kill was calculated as [(CFU_control − CFU_sample)/CFU_control] × 100.

2.9. Evaluation of Fresh Minced Pork Preservation Using LDPE-CS/Gl and LDPE-CS/Gl/CV@NZ Bilayer Films

The preservation performance of the developed bilayer films was assessed using fresh minced pork as a food matrix. Pork samples were obtained from a local meat-processing unit and immediately transported under refrigeration to the laboratory. For each treatment group—LDPE control, LDPE-CS/Gl, and LDPE-CS/Gl/CV@NZ—50 g portions of minced meat were prepared. Each sample was placed in direct contact with the inner (CS-based) surface of the corresponding bilayer film, heat-sealed to prevent any oxygen from entering (Figure 2), and stored at a constant temperature of 4 ± 1 °C for 8 days in Bosch Series 6 laboratory-grade refrigerator (Model KGNV36W31G, Bosch Hausgeräte GmbH, Stuttgart, Germany). These storage conditions represent ideal refrigerated conditions without temperature fluctuations; simulated cold chain conditions (e.g., periodic temperature abuse) were not evaluated in this study. Analyses were conducted on Days 0, 2, 4, 6, and 8 to monitor physicochemical and microbiological changes.

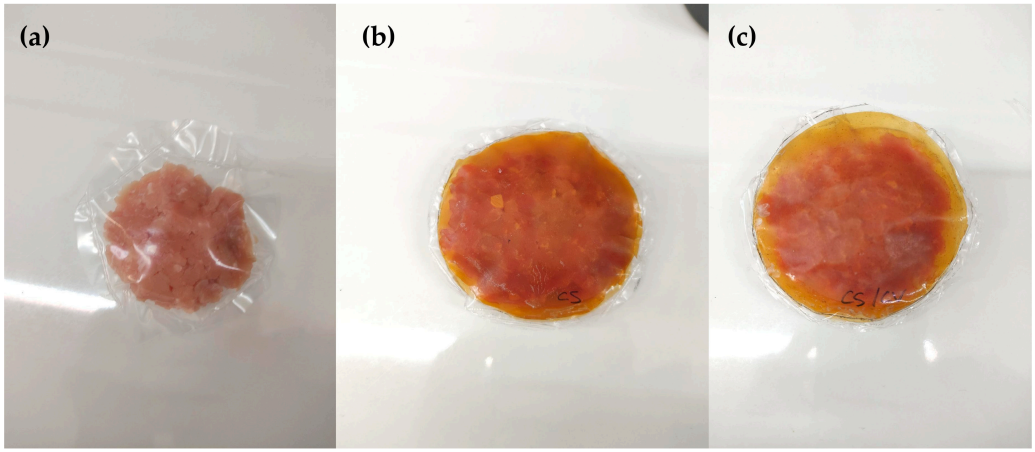


Figure 2. Packaged minced pork in heat-sealed films of (**a**) LDPE, (**b**) LDPE-CS/Gl, and (**c**) LDPE-CS/Gl/CV@NZ.

2.9.1. Physicochemical Analysis

Determination of pH

The pH of minced pork samples was measured using a digital pH meter equipped with a penetration probe and integrated temperature compensation (MW102 PRO+, Milwaukee, WI, USA). Before each measurement session, the device was calibrated using standard buffer solutions (pH 4.0 and 7.0). Each treatment was analyzed in triplicate (n = 3), and results were expressed as mean ± standard deviation (SD).

Color Assessment

Color changes on the surface of minced pork were quantified using a portable colorimeter (LS171, Linshang, Shenzhen, China) in the CIELAB color space (L^*,a^*,b^*), with

measurements taken by placing the colorimeter on the surface of the meat. Results were expressed as mean ± SD out of three replicates (n = 3).

2.9.2. Microbiological Evaluation of Active Films Using Total Viable Count (TVC) Assay

The antimicrobial efficacy of the developed LDPE-CS/Gl and LDPE-CS/Gl/CV@NZ bilayer active films was assessed against the natural microflora of fresh minced pork using the Total Viable Count (TVC) method [50,51]. This assay was conducted to simulate real-world food preservation conditions and quantify the films' ability to suppress overall microbial proliferation during refrigerated storage.

10 g of minced pork were aseptically transferred to sterile stomacher bags containing 90 mL of Buffered Peptone Water (BPW) (Biolife Italiana, Monza, Italy) and homogenized for 90 s using a Stomacher blender (BagMixer, Interscience, France). Subsequent decimal dilutions were prepared in BPW, and 0.1 mL aliquots from each dilution were spread onto plates with Plate Count Agar (PCA) (Biochem Chemopharma, Cosne Sur Loire, France). The inoculated plates were incubated at 30 °C for 72 h to allow colony development. Following incubation, colony-forming units were enumerated, and results were expressed as $\log_{10}$ CFU/g of meat sample. All analyses were performed in triplicate (n = 3) at predetermined storage intervals (days 0, 2, 4, 6, and 8).

The TVC method provides a comprehensive measure of aerobic mesophilic bacterial load, serving as a key indicator of microbiological quality and spoilage progression in perishable food products, such as minced pork. This quantitative approach enables direct comparison of the preservative efficacy between the different active film formulations (LDPE-CS/Gl and LDPE-CS/Gl/CV@NZ) and the uncoated LDPE control throughout the storage period.

Shelf-life endpoint definition: The microbiological shelf life of minced pork was defined as the storage time at which the Total Viable Count (TVC) reached or exceeded 7 log CFU/g (10^7 CFU/g), which is the generally accepted spoilage threshold for fresh meat. This criterion is based on European Commission guidelines and established food microbiology literature [52].

2.10. Statistical Analysis

All experiments were performed in triplicate, and results were expressed as mean values ± standard deviation (SD). Data normality and homogeneity of variances were verified before analysis. Statistical comparisons between multiple groups were conducted using two-way analysis of variance (ANOVA) followed by Tukey's Honestly Significant Difference (HSD) post hoc test for pairwise comparisons. Statistical significance was defined at a threshold of $p < 0.05$. All statistical analyses were performed using SPSS software (version 28.0, IBM Corporation, Armonk, NY, USA). Different superscript letters within tables and figures indicate statistically significant differences between treatments or time points, while the same letters denote no significant difference.

3. Results

3.1. ATR-FTIR Analysis of LDPE-CS/Gl and LDPE-CS/Gl/CV@NZ Films

The ATR-FTIR spectra of the pure LDPE film, the external and internal sides of the LDPE-CS/Gl bilayer film, and the external and internal sides of the LDPE-CS/Gl/CV@NZ bilayer film are presented in Figure 3 for comparative evaluation.

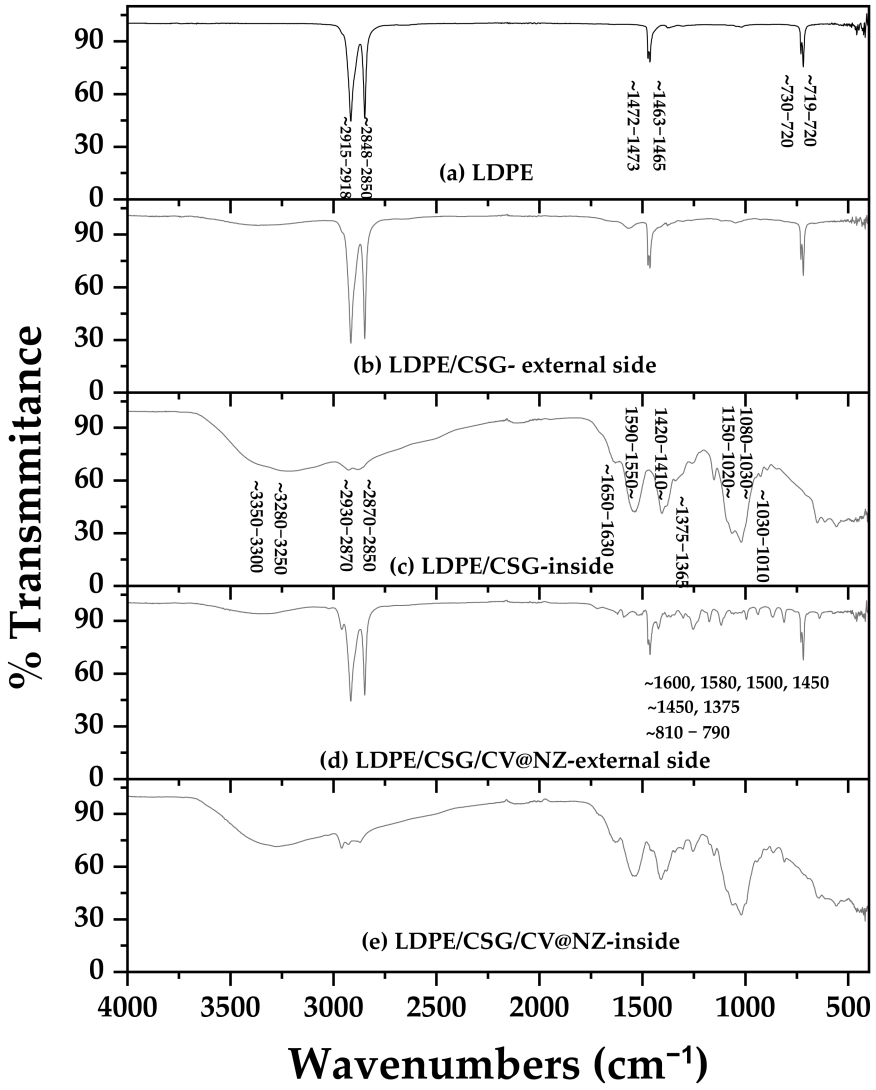


Figure 3. ATR-FTIR spectra of (**a**) neat low-density polyethylene (LDPE) film; (**b**) external side (LDPE side) of the LDPE-CS/Gl bilayer film; (**c**) internal side (CS/Gl side) of the LDPE-CS/Gl bilayer film; (**d**) external side (LDPE side) of the LDPE-CS/Gl/CV@NZ bilayer film; and (**e**) internal side (CS/Gl/CV@NZ side) of the LDPE-CS/Gl/CV@NZ bilayer film. Comparison of (**c**,**e**) reveals additional bands in (**e**) characteristic of carvacrol (e.g., aromatic C=C at 1600/1580 cm^{-1}, phenolic C–O at 1350–1250 cm^{-1}, and aromatic C–H oop at 810–790 cm^{-1}), confirming CV retention in the inner layer.

The FTIR spectrum of neat low-density polyethylene (LDPE) (Figure 3a) exhibits characteristic absorption bands corresponding to its aliphatic hydrocarbon backbone [53]. The strong absorption bands observed at approximately 2915–2918 cm^{-1} and 2848–2850 cm^{-1} are attributed to the asymmetric and symmetric stretching vibrations of methylene (CH_2) groups, respectively. In the bending region, the bands observed at 1463 cm^{-1} (CH_2 scissoring) and 1375 cm^{-1} (CH_3 symmetric bending) in the LDPE spectrum are characteristic of the polyethylene backbone and are distinct from chitosan's amide bands (1650 and 1550 cm^{-1}), confirming that no chemical reaction between LDPE and CS occurred at the interface. Notably, the characteristic doublet in the lower wavenumber region, with bands at 730–720 cm^{-1} and 719–720 cm^{-1}, corresponds to the rocking vibrations of CH_2 groups; the higher component (~730 cm^{-1}) is associated with crystalline domains, whereas the lower component (~720 cm^{-1}) originates from amorphous regions, reflecting the semi-crystalline nature of LDPE [53,54].

The ATR-FTIR spectrum recorded from the external side of the LDPE-CS/Gl bilayer film (Figure 3b) is almost identical to that of pure LDPE. However, several weak intensity peaks are discernible in the 3000–3500 cm^{-1} region and between 1700–1000 cm^{-1}. These low-intensity absorptions suggest the partial presence of chitosan components toward the outer LDPE layer, likely due to beam penetration at certain wavelengths (where ATR penetration depth exceeds the CS layer thickness) or minor thickness variations induced during hot-pressing, likely induced during the hot-pressing step [14,55–58].

The spectrum of the internal side of the LDPE-CS/Gl bilayer film (Figure 3c) displays a typical profile of a CS/Gl film [59–61]. A broad, intense absorption band centered in the 3350–3300 cm^{-1} region is observed, arising from overlapping O–H stretching vibrations of glycerol (Gl) and chitosan, together with N–H stretching from chitosan's amine and amide groups [59–61]. The aliphatic environment of the biopolymer blend is confirmed by medium-intensity C–H stretching bands between 2930 and 2850 cm^{-1} [59–61]. The presence of residual acetyl groups in chitosan is evidenced by the strong amide I (C=O stretch) band near 1650 cm^{-1} and the amide II (N–H bending) band in the 1590–1550 cm^{-1} region. Furthermore, a strong and broad composite band spanning 1150–1000 cm^{-1} is critical, as it includes the C–O–C glycosidic linkage stretch of the chitosan backbone, as well as distinct C–O stretching vibrations originating from the primary and secondary alcohol groups of the glycerol plasticizer [55,59–61].

The ATR-FTIR spectrum of the external side of the LDPE-CS/Gl/CV@NZ bilayer film (Figure 3d) exhibits the characteristic LDPE absorption pattern. Nevertheless, additional bands indicative of CV are clearly observed [62–64]. Specifically, bands in the ~1600–1450 cm^{-1} region (at approximately 1600, 1580, 1500, and 1450 cm^{-1}) are assigned to the aromatic ring C=C stretching vibrations [62–64]. The bands at ~1450 and 1375 cm^{-1} are primarily due to asymmetric and symmetric C–H bending modes of methyl ($–CH_3$) groups, respectively. A medium-intensity band in the broad region of ~1350–1250 cm^{-1} is attributed to phenolic C–O stretching. Finally, the distinctive band in the range of ~810–790 cm^{-1} corresponds to the aromatic C–H out-of-plane bending vibration, characteristic of the 1,2,4-trisubstituted benzene ring of CV. The presence of these CV-related bands on the external LDPE surface suggests that partial evaporation of CV from the inner CS/Gl/CV@NZ layer occurred during the hot-pressing process, followed by adsorption onto the outer LDPE film [62–65].

The ATR-FTIR spectrum of the internal side of the LDPE-CS/Gl/CV@NZ bilayer film (Figure 3e) shows a combination of the characteristic bands of CS, Gl, and CV, confirming the successful incorporation and retention of the CV@NZ nanohybrid within the inner bioactive layer [62].

Detailed comparison of inner-side spectra (Figure 3c vs. Figure 3e): A direct comparison of the internal side spectrum of LDPE-CS/Gl (Figure 2c) and LDPE-CS/Gl/CV@NZ (Figure 3e) reveals several distinct differences that confirm the successful incorporation and retention of CV within the inner chitosan layer, rather than complete migration to the outer LDPE surface.

The spectrum of the CV-free inner layer (Figure 3c) exhibits the characteristic bands of chitosan/glycerol: a broad O–H/N–H stretching band centered at 3350–3300 cm^{-1}, C–H stretches at 2930–2850 cm^{-1}, amide I (C=O) at ~1650 cm^{-1}, amide II (N–H) at ~1550 cm^{-1}, and the complex C–O–C/C–O band at 1150–1000 cm^{-1}.

In contrast, the CV@NZ-containing inner layer spectrum (Figure 3e) displays additional bands unequivocally assignable to carvacrol, which are absent in Figure 2c. These characteristic CV bands include:

1600, 1580, 1500, and 1450 cm^{-1}—aromatic ring C=C stretching vibrations (the doublet at 1600/1580 cm^{-1} is particularly diagnostic for substituted benzene rings);

~1375 cm^{-1}—symmetric C–H bending of the isopropyl methyl groups (CH_3);

~1350–1250 cm^{-1} (broad, medium intensity)—phenolic C–O stretching vibration;

~810–790 cm^{-1} (distinctive doublet)—aromatic C–H out-of-plane bending characteristic of a 1,2,4-trisubstituted benzene ring (the substitution pattern of carvacrol).

Evidence against complete CV migration: If CV had migrated entirely from the inner layer to the outer LDPE surface during hot-pressing, the inner layer spectrum (Figure 3e) would be indistinguishable from the CV-free spectrum (Figure 3c). The clear presence of the CV-specific bands described above in Figure 3e, with moderate to strong intensities, demonstrates that a substantial amount of CV remains within the inner chitosan/glycerol layer. Furthermore, while the outer LDPE spectrum (Figure 3d) does show weak CV bands (indicating some partial migration, as noted in the main text), the much stronger and more complete set of CV bands in the inner layer spectrum (Figure 3e) confirms that the majority of CV is retained in the intended bioactive layer. This retention is attributed to the encapsulation of CV within the zeolite nanopores and the hydrogen-bonding interactions between CV's phenolic OH group and the chitosan matrix.

Collectively, these spectral assignments provide unambiguous evidence that the CV@NZ nanohybrid is successfully incorporated and largely retained within the inner chitosan/glycerol layer of the bilayer film, despite some partial migration to the outer LDPE surface during hot-pressing.

3.2. Tensile Properties

The mechanical properties, including ultimate tensile strength (σ_{uts}) and elongation at break (%ε), of the monolayer and bilayer films are presented in Table 1. Values are expressed as mean ± standard deviation (n = 5), and superscript letters indicate statistically significant differences ($p < 0.05$) as determined by one-way ANOVA followed by Tukey's honestly significant difference (HSD) post hoc test.

Table 1. Mechanical properties (Elastic Modulus E; Ultimate Tensile Strength, σ_{uts}; Elongation at Break, %ε) of monolayer and bilayer films. Individual replicate values (n = 5) are shown in parentheses.

Film	E (MPa)	σ_{uts} (MPa)	%ε (%)
LDPE	125.3 ± 8.7 ^{d} (117.8, 134.2, 121.5, 128.6, 124.4)	12.0 ± 1.2 ^{d} (11.2, 13.5, 10.8, 12.4, 12.1)	443.3 ± 26.0 ^{a} (471.2, 421.5, 455.8, 412.4, 455.6)
CS/Gl	1850.5 ± 95.2 ^{c} (1785.3, 1962.8, 1842.6, 1905.4, 1756.4)	38.7 ± 2.0 ^{c} (36.2, 41.5, 37.9, 40.1, 37.8)	15.4 ± 3.8 ^{b} (19.1, 11.5, 18.2, 10.9, 17.3)
CS/Gl/CV@NZ	2985.7 ± 82.4 ^{a} (2912.5, 3045.8, 2978.3, 2925.6, 3066.3)	49.7 ± 1.6 ^{a} (48.2, 51.5, 49.7, 47.9, 51.2)	6.7 ± 1.2 ^{c} (5.9, 8.1, 5.2, 6.8, 7.5)
LDPE-CS/Gl	1812.3 ± 112.6 ^{c} (1675.8, 1945.6, 1778.4, 1895.2, 1766.5)	38.0 ± 5.5 ^{c} (32.5, 45.7, 36.2, 42.1, 33.5)	13.4 ± 5.6 ^{b} (19.2, 6.4, 15.8, 8.7, 16.9)
LDPE-CS/Gl/CV@NZ	2956.8 ± 145.3 ^{a,b} (2795.6, 3125.8, 2890.4, 3085.3, 2886.9)	50.0 ± 3.7 ^{a,b} (46.2, 55.1, 48.7, 52.3, 47.7)	6.6 ± 1.4 ^{c} (5.2, 8.3, 5.4, 7.9, 6.2)

Values are presented as mean ± standard deviation (n = 5). Individual replicate values are shown in parentheses below each mean. Different superscript letters (a–d) within the same column indicate statistically significant differences ($p < 0.05$) according to one-way ANOVA followed by Tukey's HSD post hoc test. Film thicknesses: LDPE = 0.06 mm; CS/Gl and CS/Gl/CV@NZ monolayers = 0.04 mm; all bilayer films = 0.10 mm (LDPE 0.06 mm + CS layer 0.04 mm).

The mechanical properties, including elastic modulus (E), ultimate tensile strength (σ_{uts}), and elongation at break (%ε), of the monolayer and bilayer films are presented in Table 1. Values are expressed as mean ± standard deviation (n = 5), and superscript letters indicate statistically significant differences ($p < 0.05$) as determined by one-way ANOVA followed by Tukey's HSD post hoc test.

One-way ANOVA revealed highly significant differences among all film groups for elastic modulus (F = 287.6, $p < 0.001$), ultimate tensile strength (F = 95.42, $p < 0.001$), and elongation at break (F = 318.6, $p < 0.001$). Subsequent post hoc analysis using Tukey's HSD test confirmed four key statistical findings.

First, neat LDPE was significantly distinct from all CS-containing groups across all three mechanical parameters, confirming the fundamental mechanical dissimilarity between the ductile polyolefin (low modulus, low strength, high elongation) and the rigid biopolymer-based systems (high modulus, high strength, low elongation). The elastic modulus of LDPE (125.3 MPa) is characteristic of a flexible, rubbery polymer above its glass transition temperature, while the substantially higher moduli of the CS-based films (1850–2985 MPa) reflect their glassy, rigid nature at ambient temperature.

Second, CS/Gl and LDPE-CS/Gl were statistically equivalent in all parameters—elastic modulus (1850.5 vs. 1812.3 MPa), tensile strength (38.7 vs. 38.0 MPa), and elongation (15.4% vs. 13.4%)—demonstrating that the corona treatment and hot-pressing procedure successfully preserved the mechanical integrity of the CS layer without inducing thermal degradation, delamination, or disruption of the biopolymer's inherent stiffness.

Third, CS/Gl/CV@NZ and LDPE-CS/Gl/CV@NZ were statistically equivalent across all properties, confirming that the reinforcing effect imparted by the CV@NZ nanohybrid was fully retained following the bilayer assembly process. The elastic modulus increased dramatically from approximately 1850 MPa to approximately 2970 MPa upon nanohybrid incorporation—a 60% enhancement that unequivocally confirms the stiffening effect of the rigid inorganic filler.

Fourth, all CV@NZ-containing groups exhibited significantly higher elastic modulus (≈2970 MPa vs. ≈1850 MPa), significantly higher tensile strength (≈50 MPa vs. ≈38 MPa), and significantly lower elongation (≈6.6% vs. ≈14.5%) compared to their neat CS/Gl counterparts. This pattern unequivocally confirms the reinforcing and concomitant embrittling effect of the nanohybrid filler, consistent with classic composite theory where rigid inclusions increase stiffness and strength at the expense of ductility.

The statistical equivalence between monolayer and corresponding bilayer films constitutes the most mechanistically significant finding of the mechanical characterization. This equivalence provides robust evidence that interfacial adhesion achieved via corona surface activation—operating at ambient pressure with an optimized treatment intensity of 0.75 s/cm^2 at 45 kV and 30 W—was sufficient to prevent premature failure at the LDPE-CS interface during tensile loading. Furthermore, the applied hot-pressing conditions (110 °C, 1 min, 1 ton) did not induce complete thermal volatilization of CV, as evidenced by the strong CV-specific bands in the inner layer FTIR spectrum (Figure 3e). However, partial evaporation and migration of a small fraction of CV to the outer LDPE surface were observed (Figure 3d), indicating that the zeolite carrier effectively retains the majority of CV within the inner layer while allowing some surface equilibration, structural degradation of the NZ framework, or disruption of the chitosan-glycerol hydrogen bonding network. From an industrial perspective, this statistical equivalence is particularly critical, as it demonstrates that the functional performance of the bioactive nanohybrid is fully transferable from laboratory-scale solution-cast monolayers to industrially relevant bilayer configurations. One-way ANOVA confirmed that the LDPE-CS/Gl/CV@NZ group was statistically distinct from the neat CS/Gl and LDPE-CS/Gl groups in elastic

modulus ($p < 0.001$) and tensile strength ($p < 0.001$), while showing equivalence to the CS/Gl/CV@NZ monolayer ($p > 0.05$). The reference for statistical equivalence is the corresponding CS-based monolayer (CS/Gl or CS/Gl/CV@NZ), not LDPE. This confirms that the bilayer assembly process does not alter the intrinsic mechanical properties of the bioactive layer. The complete ANOVA results (F-values and *p*-values) are reported at the bottom of Table 1.

The restricted chain mobility induced by the nanohybrid is directly evidenced by the significant reduction in elongation at break, which decreased from 15.4% to 6.7% in monolayers and from 13.4% to 6.6% in bilayers. This inverse relationship between stiffness (modulus) and extensibility represents a well-documented trade-off in nanoparticle-reinforced polymer composites and confirms that the CV@NZ nanohybrid functions as an effective mechanical reinforcement agent rather than merely an inert additive [14,18]. The approximately 60% increase in modulus, coupled with a 60% decrease in elongation, demonstrates the classic stiffness-ductility balance observed in filled polymer systems.

The elongation behavior of the bilayer films warrants particular mechanistic interpretation. Both LDPE-CS/Gl and LDPE-CS/Gl/CV@NZ bilayer films exhibited elongation values statistically indistinguishable from their respective monolayer controls (13.4% vs. 15.4% for non-reinforced; 6.6% vs. 6.7% for reinforced), despite the presence of the highly extensible LDPE substrate (443.3% elongation). This observation demonstrates that, under uniaxial tensile loading, mechanical failure initiates and propagates exclusively within the brittle chitosan-based layer well before the ductile LDPE substrate reaches its yield point. The LDPE layer, therefore, does not contribute to the overall elongation of the bilayer system. This phenomenon is characteristic of rigid-on-ductile multilayer configurations where a substantial mechanical property mismatch exists between the two components [66]. Critically, the absence of delamination or interfacial slippage during tensile testing—evidenced by the retention of monolayer-equivalent tensile strength and modulus in the bilayers—confirms that corona treatment provided sufficient surface activation to maintain adhesive integrity, even though it could not overcome the intrinsic brittleness of the chitosan-based layer. From a packaging functionality perspective, this behavior is acceptable, as the LDPE substrate remains available to provide moisture barrier, heat-sealability, and structural integrity; however, the overall bilayer flexibility (measured as elongation at break) is dictated by the brittle chitosan layer, not the ductile LDPE substrate during converting operations and end-use handling, while the CS-based inner layer is hypothesized to supply the targeted high oxygen barrier and bioactive functionality, which will be confirmed in the following sections.

During tensile testing, the chitosan layer exhibited visible crazing and micro-cracking prior to failure, while the LDPE layer remained intact and elastically deformed. No delamination was observed at the LDPE-CS interface, confirming the effectiveness of the corona treatment. Representative stress–strain curves are provided in Supplementary Figure S1.

The mechanical property profile of the developed bilayer films aligns favorably with the performance requirements of high-barrier active packaging applications. Although elongation is substantially reduced compared to neat LDPE, tensile strength is more than quadrupled (from 12.0 MPa to 50.0 MPa), and elastic modulus is increased by more than an order of magnitude (from 125 MPa to ≈2950 MPa), providing enhanced resistance to mechanical stresses encountered during form-fill-seal operations, transportation vibration, compression during stacking, and consumer handling. The high modulus ensures dimensional stability and resistance to deformation under load—critical properties for maintaining package integrity and barrier performance throughout the supply chain. The statistical robustness of the mechanical data—supported by low standard deviations and

clear separation of treatment groups—further confirms the reproducibility and reliability of the developed fabrication protocol.

Collectively, these mechanical results demonstrate that the proposed corona-assisted bilayer assembly strategy successfully combines the complementary properties of synthetic LDPE and biobased chitosan without compromising the performance of either component. The incorporation of the CV@NZ nanohybrid provides substantial reinforcement (60% modulus increase, 30% strength increase) while maintaining the statistical equivalence between monolayer and bilayer configurations, confirming the industrial viability of the approach. This represents a significant advancement toward the development of industrially scalable, high-performance active packaging materials that align with circular economy principles by minimizing biopolymer usage while maximizing functional output.

3.3. Oxygen Barrier Properties

The oxygen barrier properties of neat LDPE and the bilayer films were evaluated by measuring the Oxygen Transmission Rate (OTR) and calculating the Oxygen Permeability (PeO_2). Table 2 presents the film thickness, OTR, and PeO_2 values for LDPE, LDPE-CS/Gl, and LDPE-CS/Gl/CV@NZ films. Values are expressed as mean ± standard deviation (n = 5), and superscript letters indicate statistically significant differences ($p < 0.05$) as determined by one-way ANOVA followed by Tukey's HSD post hoc test.

Table 2. Oxygen barrier properties (Oxygen Transmission Rate, OTR; Oxygen Permeability, PeO_2) of LDPE and bilayer films.

Film	Film Thickness (mm)	OTR (cc/m^2·Day)	PeO_2 ($\times 10^{-11}$ cm^2/s)
LDPE	0.06 ± 0.01	667.0 ± 5.8 ^{a}	46.50 ± 0.40 ^{a}
LDPE-CS/Gl	0.10 ± 0.01	10.4 ± 0.2 ^{c}	1.20 ± 0.02 ^{c}
LDPE-CS/Gl/CV@NZ	0.10 ± 0.01	18.5 ± 0.3 ^{b}	2.14 ± 0.03 ^{b}

Values are presented as mean ± standard deviation (n = 5). Different superscript letters (a–c) within the same column indicate statistically significant differences ($p < 0.05$) according to one-way ANOVA followed by Tukey's HSD post hoc test. Fold reductions are calculated from PeO_2 values relative to neat LDPE (46.5 × 10^{-11} cm^2/s). One-way ANOVA confirmed highly significant differences among all film groups for both OTR (F = 38,426.8, $p < 0.001$) and PeO_2 (F = 38,511.2, $p < 0.001$).

One-way ANOVA revealed highly significant differences among all film groups for both OTR (F = 38,426.8, $p < 0.001$) and PeO_2 (F = 38,511.2, $p < 0.001$). The fold reductions reported herein are calculated using PeO_2 values relative to neat LDPE (46.50 × 10^{-11} cm^2/s).

Neat LDPE exhibited an OTR of 667.0 ± 5.8 cc/m^2·day and a PeO_2 of 46.50 ± 0.40 × 10^{-11} cm^2/s. The LDPE-CS/Gl bilayer film achieved an OTR of 10.4 ± 0.2 cc/m^2·day and a PeO_2 of 1.20 ± 0.02 × 10^{-11} cm^2/s, corresponding to a 39-fold reduction in oxygen permeability. The LDPE-CS/Gl/CV@NZ bilayer film exhibited an OTR of 18.5 ± 0.3 cc/m^2·day and a PeO_2 of 2.14 ± 0.03 × 10^{-11} cm^2/s, corresponding to a 22-fold reduction.

The superior oxygen barrier of the LDPE-CS/Gl film is attributed to the dense hydrogen-bonded network and high crystallinity of chitosan, which create a highly tortuous pathway for oxygen diffusion. This tortuosity effect can be understood through percolation theory, which describes how dispersed impermeable domains (crystalline regions of chitosan) force diffusing gas molecules to follow longer paths around these obstacles, effectively reducing permeability [67]. In the chitosan matrix, the hydrogen-bonded network acts as a semi-continuous barrier phase, increasing the diffusional path length by a factor proportional to the aspect ratio and volume fraction of the crystalline domains.

The modest but statistically significant increase in oxygen permeability upon CV@NZ incorporation (from 1.20 to 2.14 × 10^{-11} cm^2/s, $p < 0.05$) reflects two competing factors.

First, the rigid zeolite nanoparticles disrupt the chitosan hydrogen-bonded network, creating localized free volume that facilitates gas diffusion—a phenomenon consistent with the "anti-percolation" effect where rigid fillers can either enhance or reduce barrier properties depending on their dispersion state and interfacial compatibility. Second, carvacrol exerts a plasticization effect, increasing polymer chain mobility and free volume, which further elevates oxygen transport. Despite this modest increase (approximately 1.8-fold relative to the neat chitosan bilayer), the LDPE-CS/Gl/CV@NZ film still maintains excellent barrier performance (22-fold reduction vs. neat LDPE), which is fully compatible with modified atmosphere packaging requirements for oxygen-sensitive foods such as fresh meat and poultry.

The low coefficients of variation (<3% for all groups) confirm the reproducibility of the bilayer fabrication protocol. These results demonstrate that a thin (40 μm) chitosan-based layer can elevate LDPE from "poor" to "high-barrier" classification, while the CV@NZ nanohybrid retains sufficient barrier performance for active packaging applications.

3.4. Antioxidant Activity

The antioxidant capacity of the bilayer films, arising from the incorporated chitosan and CV@NZ nanohybrid, was evaluated using the DPPH radical scavenging assay. The calculated EC_{50} values (the concentration required to scavenge 50% of DPPH radicals) for the LDPE-CS/Gl and LDPE-CS/Gl/CV@NZ films are presented in Table 3.

Table 3. Antioxidant activity (EC_{50}, DPPH) of LDPE-CS/Gl and LDPE-CS/Gl/CV@NZ bilayer films.

Film	EC_{50}, DPPH (mg/mL)
LDPE	- *
LDPE-CS/Gl	216.16 ± 18.96 [a]
LDPE-CS/Gl/CV@NZ	13.49 ± 1.07 [b]

Values are presented as mean ± standard deviation (n = 3). Different superscript letters (a, b) indicate statistically significant differences ($p < 0.001$) according to one-way ANOVA. * The neat LDPE film exhibited no antioxidant activity, as it lacks radical-scavenging components, and was therefore excluded from the statistical analysis. The LDPE-CS/Gl/CV@NZ film showed significantly higher antioxidant activity (F = 359.7, $p < 0.001$) compared to LDPE-CS/Gl.

It should be noted that EC_{50} values are expressed per mass of film. Since the active surface area in contact with the DPPH solution is identical for monolayer and bilayer films (only the inner CS layer contacts the solution), direct comparison between formulations is valid. However, future studies should consider normalizing to active surface area (mg/cm^2) for true intrinsic activity comparisons between different film architectures.

The statistical analysis revealed a highly significant difference ($p < 0.001$, F = 359.7) in antioxidant activity between the two bilayer film formulations. The LDPE-CS/Gl film exhibited a high EC_{50} value of 216.16 ± 18.96 mg/mL, indicating a relatively low antioxidant capacity. This baseline activity is attributed solely to the chitosan (CS) matrix, which is known to possess moderate radical-scavenging properties due to the presence of free amino and hydroxyl groups that can react with free radicals [11,59].

In stark contrast, the LDPE-CS/Gl/CV@NZ film demonstrated a dramatically lower EC_{50} value of 13.49 ± 1.07 mg/mL. This represents approximately a 16-fold increase in antioxidant potency compared to the film without the nanohybrid. This substantial enhancement is unequivocally attributed to the successful incorporation of the CV@NZ nanohybrid. CV, a phenolic monoterpene, is a potent antioxidant that acts as a powerful radical scavenger by donating hydrogen atoms or electrons [62,65]. The NZ serves as an effective carrier, facilitating the dispersion and retention of CV within the chitosan matrix. The EC_{50} value of 13.49 mg/mL for the LDPE-CS/Gl/CV@NZ film aligns favorably with other CV-based active packaging systems reported in the literature, confirming its strong

potential to inhibit oxidative degradation in packaged foods, such as lipid oxidation in fatty meats or nuts [62]. The low standard deviation for this sample (1.07) further confirms the homogeneity of the CV@NZ dispersion within the film.

3.5. Antibacterial Activity

The antibacterial activity of the tested films is presented in Table 4, expressed as logCFU/g. All experiments were performed in triplicate (n = 3) under the conditions described in Section 2.8: contact time of 24 h at 37 °C, initial bacterial concentration of approximately 1–2 × 10^9 CFU/mL (control values of 9.89 ± 0.22 log CFU/g for *L. monocytogenes* and 9.61 ± 0.12 log CFU/g for *E. coli*).

Table 4. Antibacterial activity of LDPE, LDPE-CS/Gl and LDPE-CS/Gl/CV@NZ films in comparison to control samples (pure bacteria cultures) against *Listeria monocytogenes* and *Escherichia coli* expressed as log CFU/g.

Microorganism/logCFU/g	Control	LDPE	LDPE-CS/Gl	LDPE-CS/Gl/CV@NZ
Listeria monocytogenes	9.89 ± 0.22 ^{a}	9.47 ± 0.31 ^{a,d}	9.05 ± 0.04 ^{b,d,f}	4.81 ± 0.20 ^{c,e,g}
Escherichia coli	9.61 ± 0.12 ^{h}	9.30 ± 0.33 ^{h,k}	8.29 ± 0.04 ^{i,l,n}	4.31 ± 0.31 ^{j,m,o}

Values are mean ± SD (n = 3). Different superscript letters in the same row indicate statistically significant differences ($p < 0.05$, one-way ANOVA with Tukey's HSD post hoc test). The percent kill for LDPE-CS/Gl/CV@NZ was >99.999% for both bacterial strains.

One-way ANOVA confirmed significant differences among the four treatment groups for both *L. monocytogenes* (F = 124.7, $p < 0.001$) and *E. coli* (F = 98.3, $p < 0.001$). Post hoc comparisons (Tukey's HSD) are indicated by superscript letters in Table 4. Regarding *Listeria monocytogenes*, the control sample presented a value of 9.89 ± 0.22 log CFU/g, while the LDPE film in contact with the Petri dish showed a value of 9.47 ± 0.31 log CFU/g, which was statistically equivalent to the control sample ($p > 0.05$), confirming that unmodified LDPE possesses no intrinsic antibacterial activity. The incorporation of the CS/Gl layer resulted in a significantly lower value of 9.05 ± 0.04 log CFU/g ($p < 0.05$ compared to control), representing approximately a 0.8 log reduction. This modest but statistically significant antibacterial effect is attributed to the intrinsic antimicrobial properties of chitosan. A substantially more pronounced decrease was observed for the LDPE-CS/Gl/CV@NZ film, with a value of 4.81 ± 0.20 log CFU/g—representing a 5.08 log reduction compared to the control (from 9.89 to 4.81 log CFU/g), which corresponds to >99.999% bacterial kill (specifically 99.9991% calculated as $[(10^{9.89} - 10^{4.81})/10^{9.89}] \times 100$). This dramatic enhancement demonstrates the potent synergistic effect of combining chitosan with the CV-loaded zeolite nanohybrid.

Regarding *Escherichia coli*, the control sample showed a value of 9.61 ± 0.12 log CFU/g, and the pure LDPE film exhibited a statistically similar value (9.30 ± 0.33 log CFU/g, $p > 0.05$). The incorporation of CS/Gl resulted in a significantly lower value of 8.29 ± 0.04 log CFU/g (approximately 1.3 log reduction), which was significantly different from both the control and the LDPE film. In the case of LDPE-CS/Gl/CV@NZ, a substantial decrease to 4.31 ± 0.31 log CFU/g was observed—a 5.30 log reduction compared to the control (from 9.61 to 4.31 log CFU/g), corresponding to >99.999% bacterial kill (specifically 99.9995%, calculated as $[(10^{9.61} - 10^{4.31})/10^{9.61}] \times 100$). Representative Petri dish images showing the substantial reduction in bacterial colonies for both E. coli and L. monocytogenes after exposure to the LDPE-CS/Gl/CV@NZ film are presented in Figure 4.

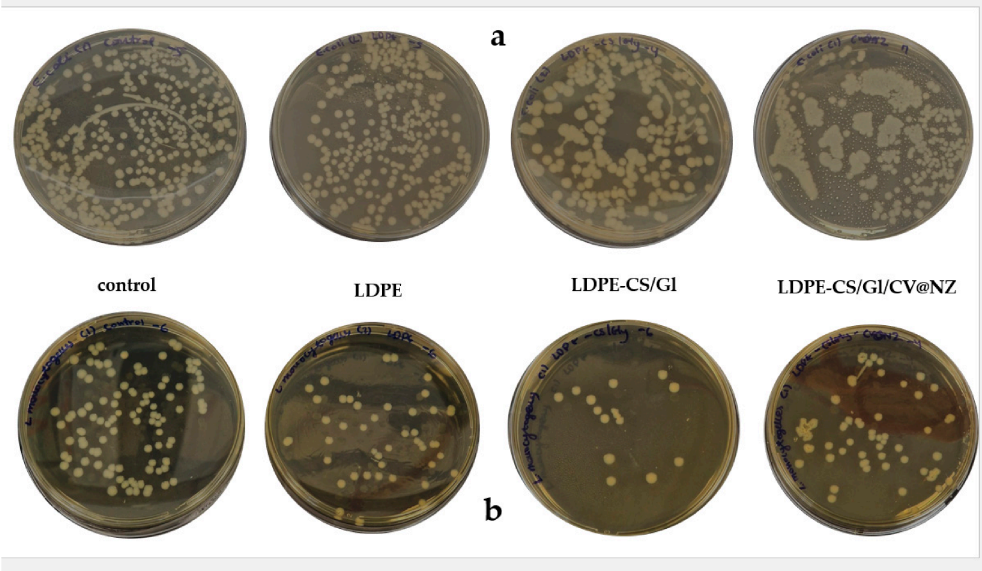


Figure 4. Representative Petri dishes showing colony formation at different dilutions for (**a**) *Escherichia coli* and (**b**) *Listeria monocytogenes* after exposure to different film samples. The plates correspond to the control, LDPE, LDPE-CS/Gl, and LDPE-CS/Gl/CV@NZ treatments. For *Escherichia coli*, the dilutions are 10^{-6} g/mL, 10^{-6} g/mL, 10^{-5} g/mL, 10^{-2} g/mL, respectively; meanwhile, the Listeria monocytogenes are 10^{-6} g/mL in the first 3 samples and 10^{-5} g/mL in the last sample.

The antimicrobial efficacy of the CS/Gl film (without nanohybrid) was notably higher against *E. coli* (1.3 log reduction) compared to *L. monocytogenes* (0.8 log reduction). This differential susceptibility aligns with the established mechanism of chitosan's antimicrobial action. Chitosan is a cationic polysaccharide that can strongly interact via electrostatic forces and hydrogen bonding with the anionic cell wall components of bacteria [68]. The outer membrane of Gram-negative bacteria such as *E. coli* contains lipopolysaccharides (LPS) with negatively charged phosphate groups, providing abundant binding sites for the protonated amino groups (NH_3^+) of chitosan. This interaction disrupts membrane integrity, increases permeability, and ultimately leads to cell death. In contrast, Gram-positive bacteria like *L. monocytogenes* possess a thick peptidoglycan layer that, while also negatively charged, presents a more robust physical barrier that may partially mitigate the membrane-disruptive effects of chitosan. The greater susceptibility of *E. coli* observed in this study is consistent with numerous reports in the literature documenting enhanced chitosan activity against Gram-negative pathogens.

The incorporation of the CV@NZ nanohybrid into the chitosan matrix leads to dramatically enhanced antibacterial activity, with approximately 5 log reductions (>99.999% kill) against both bacterial strains. CV (5-isopropyl-2-methylphenol) is a monoterpene phenolic compound and a major component of many essential oils (e.g., oregano, thyme) with well-documented broad-spectrum biological activities [69]. Owing to its amphiphilic chemical structure—combining hydrophobic characteristics from the aromatic ring with hydrophilic properties from the phenolic OH group—CV demonstrates multiple mechanisms of antibacterial action. The primary mechanism involves partitioning into the lipid bilayer of bacterial membranes, disrupting membrane integrity, increasing fluidity and permeability, causing leakage of intracellular contents (ions, ATP, nucleic acids), and ultimately leading to cell lysis [69]. Additionally, CV can inhibit bacterial quorum sensing, reduce motility, and interfere with energy metabolism.

The NZ serves a critical multifunctional role in this system. First, as a microporous aluminosilicate mineral with high surface area and cation exchange capacity, NZ acts as an effective carrier for CV, facilitating its dispersion within the chitosan matrix and

protecting it from volatilization during film processing [70]. Second, the zeolite framework enables controlled release of CV, extending the duration of antimicrobial activity. Third, the hierarchical pore structure of NZ may provide additional surface area for bacterial adhesion, bringing microorganisms into close proximity with the immobilized CV. This combination of adsorption capacity and controlled release makes zeolite a highly effective inorganic carrier for essential oil components in active packaging applications.

Importantly, the antibacterial activity of the LDPE-CS/Gl/CV@NZ film (≈5 log reduction) is markedly higher than that of the CS/Gl film alone (0.8–1.3 log reduction). This substantial enhancement suggests a synergistic interaction between chitosan and the CV@NZ nanohybrid. Several mechanisms may contribute to this synergy, including membrane destabilization by chitosan facilitating greater penetration of carvacrol, local concentration enhancement via controlled release from zeolite, and dual-target attack on bacterial cells.

Membrane destabilization: Chitosan's initial interaction with the bacterial cell wall increases membrane permeability, facilitating greater penetration of CV into the cytoplasmic membrane.

Local concentration enhancement: The zeolite particles may concentrate CV at the bacterial cell surface through local release, creating a high effective concentration at the site of action.

Sequential attack: Chitosan compromises the outer membrane (in Gram-negatives) or peptidoglycan layer (in Gram-positives), allowing CV to more readily access and disrupt the inner cytoplasmic membrane.

Metabolic disruption: Chitosan can chelate metal ions essential for bacterial enzyme function, while CV interferes with proton motive force and ATP synthesis—multiple simultaneous attacks that overwhelm bacterial defense mechanisms.

Many studies have reported enhanced antimicrobial properties following the incorporation of CV or CV-rich essential oils into polymer matrices. Brahmi et al. [56] demonstrated that CV-clay hybrids incorporated into alginate-chitosan microcapsules significantly enhanced antimicrobial activity against both Gram-negative and Gram-positive pathogens, with the clay component providing sustained release and protection of the volatile essential oil. Their findings align closely with the present study, confirming that clay minerals (including zeolites) are effective carriers for stabilizing and delivering phenolic antimicrobial compounds. Moreover, Pajnik et al. [57] reported comparable results for zeolite/chitosan/gelatin films processed with supercritical CO_2. Their study showed that films without thymol or CV exhibited negligible antibacterial activity, while incorporation of these phenolic compounds (at loadings comparable to the present study) significantly enhanced antibacterial properties against both *Escherichia coli* and *Staphylococcus aureus*, with reductions of 4–5 log CFU/mL. The present results extend these findings by demonstrating that the CV@NZ nanohybrid retains full bioactivity when incorporated into a bilayer configuration with LDPE, and that corona treatment and hot-pressing do not compromise the antimicrobial efficacy of the system.

The 5.08–5.30 log reductions observed (equivalent to >99.999% bacterial kill) represent exceptional antibacterial efficacy that meets or exceeds the performance criteria for active antimicrobial packaging materials. This level of reduction is sufficient to prevent biofilm formation, inhibit spoilage organism proliferation, and suppress pathogenic bacteria that may contaminate food surfaces. The slightly greater reduction against *E. coli* (5.3 log) compared to *L. monocytogenes* (5.1 log) likely reflects the combined susceptibility to both chitosan (preferentially active against Gram-negatives) and CV (broad-spectrum but with Gram-positive susceptibility sometimes requiring slightly higher concentrations).

These findings provide compelling evidence for the potential application of LDPE-CS/Gl/CV@NZ bilayer films as active antimicrobial packaging materials. The 5-log reduction in bacterial counts corresponds to a sterilization-level effect under the test conditions, suggesting that these films could substantially extend the shelf life of perishable foods by suppressing both spoilage and pathogenic microorganisms. The controlled release of CV from the zeolite carrier ensures that antimicrobial activity is sustained over time, while the chitosan matrix provides immediate contact killing. This dual-mode action—combining contact-active (chitosan) and release-active (CV) antimicrobial mechanisms—represents a sophisticated approach to food preservation that is particularly valuable for high-risk products such as fresh meat, poultry, and ready-to-eat foods.

The statistical robustness of the antibacterial data (low standard deviations, clear separation between treatment groups) confirms the reproducibility and reliability of the antimicrobial performance. From an industrial perspective, the retention of full antibacterial activity after corona treatment and hot-pressing demonstrates that the CV@NZ nanohybrid is sufficiently stable to withstand the thermal and mechanical stresses of film conversion processes, supporting the commercial viability of this active packaging technology.

While the contact-based antimicrobial assay provides clear evidence of bactericidal activity, future studies should investigate the kinetics of CV release from the CV@NZ nanohybrid, the migration behavior into food simulants, and the long-term stability of antimicrobial activity under realistic storage conditions. Additionally, mechanistic studies using fluorescence microscopy or electron microscopy could provide visual confirmation of the membrane disruption mechanisms proposed herein. These findings provide useful insights for the development of antimicrobial film materials with potential applications in food packaging and related industries.

3.6. Packaged Minced Pork Preservation Test

3.6.1. Physicochemical Parameters

The changes in pH and color parameters (L*, a*, b*) of minced pork packaged in LDPE, LDPE-CS/Gl, and LDPE-CS/Gl/CV@NZ films during 8 days of refrigerated storage are presented in Table 5. Two-way ANOVA revealed that both film type and storage day had a significant effect ($p < 0.05$) on all physicochemical parameters measured.

Table 5. Changes in pH of fresh minced pork packaged in LDPE, LDPE-CS/Gl, and LDPE-CS/Gl/CV@NZ films and stored at 4 °C for 8 days.

Film	Day 0	Day 2	Day 4	Day 6	Day 8
LDPE	$5.62 \pm 0.02^{a,1}$	$5.66 \pm 0.01^{ab,1}$	$5.66 \pm 0.03^{ab,1}$	$5.71 \pm 0.02^{bc,1}$	$5.72 \pm 0.01^{c,1}$
LDPE-CS/Gl	$5.62 \pm 0.02^{a,1}$	$5.52 \pm 0.02^{b,2}$	$5.37 \pm 0.02^{c,2}$	$5.46 \pm 0.03^{d,2}$	$5.48 \pm 0.06^{d,2}$
LDPE-CS/Gl/CV@NZ	$5.62 \pm 0.02^{a,1}$	$5.53 \pm 0.01^{b,2}$	$5.50 \pm 0.02^{b,3}$	$5.45 \pm 0.01^{c,2}$	$5.42 \pm 0.02^{c,3}$

Values are mean ± SD ($n = 3$). Different superscript letters (a–d) in the same row indicate significant differences between days for the same film ($p < 0.05$). Different superscript numbers (1–3) in the same column indicate significant differences between films on the same day ($p < 0.05$, two-way ANOVA, Tukey's HSD).

Two-way ANOVA revealed that both film type and storage day had significant effects on pH ($F_{film} = 34.2$, $p < 0.001$; $F_{day} = 28.7$, $p < 0.001$), redness a* ($F_{film} = 18.5$, $p < 0.01$; $F_{day} = 42.1$, $p < 0.001$), and yellowness b* ($F_{film} = 12.3$, $p < 0.05$; $F_{day} = 35.6$, $p < 0.001$). The initial pH of the minced pork was 5.62. For samples packaged in neat LDPE, the pH increased progressively throughout the storage period, reaching 5.72 on day 8. This increase is typical of meat spoilage due to the production of volatile bases and amines by microbial activity. In contrast, the pH of samples packaged with LDPE-CS/Gl and LDPE-CS/Gl/CV@NZ films decreased during the first 4–6 days before stabilizing. This initial decrease is likely due to the dissolution of CO_2, which has a high barrier in the

chitosan layer, or the acidic nature of the chitosan film-forming solution (acetic acid). By day 8, the pH of pork in LDPE-CS/Gl (5.48) and LDPE-CS/Gl/CV@NZ (5.42) was significantly lower ($p < 0.05$) than that of the LDPE control, indicating a retardation of microbial spoilage processes.

The changes in color parameters (L, a, b) of minced pork during refrigerated storage are presented in Table 6. Color is a critical quality attribute for consumer acceptance. The lightness (L) value fluctuated across all samples, with no clear trend driven by the packaging film. The redness (a) value, which is the most important color parameter for meat, decreased for all samples over time, indicating a loss of the bright red oxymyoglobin pigment. However, the decrease in a* was significantly delayed ($p < 0.05$) by the active films. On day 8, the a* value for the LDPE-CS/Gl/CV@NZ film (9.93) was significantly higher than that for the LDPE control (7.41), suggesting that the antioxidant activity of the CV helped slow down myoglobin oxidation. The yellowness (b*) value increased steadily for the LDPE control, while it remained relatively stable for the samples in contact with the chitosan-based films, further indicating the protective effect of the coatings.

Table 6. Changes in color parameters (L, a, b*) of fresh minced pork packaged in LDPE, LDPE-CS/Gl, and LDPE-CS/Gl/CV@NZ films and stored at 4 °C for 8 days.

Parameter	Film	Day 0	Day 2	Day 4	Day 6	Day 8
L*	LDPE	$50.39 \pm 2.38^{a,1}$	$56.05 \pm 1.27^{ab,1}$	$61.05 \pm 2.61^{b,1}$	$50.85 \pm 3.35^{a,1}$	$56.95 \pm 1.35^{ab,1}$
	LDPE-CS/Gl	$50.39 \pm 2.39^{a,1}$	$52.37 \pm 5.41^{a,1}$	$60.94 \pm 0.91^{b,1}$	$54.28 \pm 2.70^{ab,1}$	$54.23 \pm 1.46^{ab,1}$
	LDPE-CS/Gl/CV@NZ	$50.39 \pm 2.40^{a,1}$	$53.98 \pm 1.53^{ab,1}$	$56.86 \pm 2.61^{b,1}$	$59.60 \pm 3.45^{ab,1}$	$56.93 \pm 2.58^{ab,1}$
a*	LDPE	$14.53 \pm 0.43^{a,1}$	$10.80 \pm 0.74^{b,1}$	$9.46 \pm 0.40^{bc,1}$	$8.22 \pm 1.50^{c,1}$	$7.41 \pm 1.44^{c,1}$
	LDPE-CS/Gl	$14.53 \pm 0.43^{a,1}$	$12.45 \pm 0.98^{ab,2}$	$11.83 \pm 2.21^{ab,1}$	$9.01 \pm 1.34^{bc,1}$	$8.84 \pm 0.64^{bc,1,2}$
	LDPE-CS/Gl/CV@NZ	$14.53 \pm 0.43^{a,1}$	$13.39 \pm 0.37^{ab,2}$	$12.75 \pm 1.01^{b,1}$	$10.03 \pm 1.22^{c,1}$	$9.93 \pm 0.39^{c,2}$
b*	LDPE	$11.52 \pm 0.76^{a,1}$	$13.89 \pm 1.28^{ab,1}$	$14.62 \pm 1.12^{b,1}$	$16.52 \pm 1.17^{bc,1}$	$17.51 \pm 0.58^{c,1}$
	LDPE-CS/Gl	$11.52 \pm 0.76^{a,1}$	$12.83 \pm 0.38^{ab,1}$	$14.38 \pm 0.34^{b,1}$	$13.98 \pm 0.94^{ab,1}$	$12.85 \pm 0.28^{ab,2}$
	LDPE-CS/Gl/CV@NZ	$11.52 \pm 0.76^{a,1}$	$11.82 \pm 1.74^{a,1}$	$13.80 \pm 0.97^{ab,1}$	$13.93 \pm 2.75^{ab,1}$	$14.41 \pm 1.22^{b,2}$

Values are mean ± SD ($n = 3$). Different superscript letters (a–c) in the same row for each parameter indicate significant differences between days for the same film ($p < 0.05$). Different superscript numbers (1, 2) in the same column for each parameter indicate significant differences between films on the same day ($p < 0.05$, two-way ANOVA, Tukey's HSD).

3.6.2. Microbiological Assessment

The antimicrobial efficacy of the developed films was evaluated by monitoring the Total Viable Count (TVC) in minced pork over the 8-day storage period (Table 7). This real-food application study complements the in vitro antibacterial activity results presented in Section 3.5, providing a comprehensive assessment of film performance under practical refrigerated storage conditions.

Two-way ANOVA confirmed significant effects of film type ($F = 187.3$, $p < 0.001$) and storage day ($F = 245.6$, $p < 0.001$) on TVC, with a significant interaction term ($F = 28.4$, $p < 0.001$). The initial TVC of the minced pork was 4.75 log CFU/g, indicating good quality fresh meat suitable for shelf-life studies. Throughout the 8-day refrigerated storage period, all chitosan-coated films significantly inhibited microbial proliferation compared to the neat LDPE control, with the extent of inhibition correlating directly with the antibacterial potency established in the in vitro assays (Section 3.5).

The meat packaged in neat LDPE showed a rapid and progressive increase in TVC throughout storage. By day 2, the TVC had already increased to 6.08 log CFU/g, and by day 8, it reached 7.97 log CFU/g, substantially exceeding the typical spoilage threshold of 7 log CFU/g for fresh meat. This rapid microbial proliferation is consistent with the complete absence of antibacterial activity in unmodified LDPE, as demonstrated in Table 4, where LDPE showed statistically equivalent bacterial counts to the control against both *L. monocytogenes* (9.47 vs. 9.89 log CFU/g) and *E. coli* (9.30 vs. 9.61 log CFU/g). The LDPE

control provides no active inhibition, allowing the natural meat microflora—predominantly psychrotrophic spoilage organisms such as *Pseudomonas* spp., *Brochothrix thermosphacta*, and lactic acid bacteria—to grow unimpeded.

Table 7. Changes in Total Viable Count (TVC, log CFU/g) of fresh minced pork packaged in LDPE, LDPE-CS/Gl, and LDPE-CS/Gl/CV@NZ films and stored at 4 °C for 8 days. Individual replicate values (n = 3) are shown in parentheses.

Film	Day 0	Day 2	Day 4	Day 6	Day 8
LDPE	4.75 ± 0.01 ^{a,1} (4.76, 4.73, 4.75)	6.08 ± 0.03 ^{b,1} (6.12, 6.05, 6.08)	6.10 ± 0.42 ^{b,1} (6.61, 5.58, 6.10)	6.64 ± 0.40 ^{b,1} (7.13, 6.15, 6.64)	7.97 ± 0.01 ^{c,1} (7.98, 7.95, 7.97)
LDPE-CS/Gl	4.75 ± 0.01 ^{a,1} (4.76, 4.73, 4.75)	5.04 ± 0.46 ^{ab,2} (5.60, 4.48, 5.04)	5.17 ± 0.38 ^{ab,1,2} (5.69, 4.78, 5.04)	5.83 ± 0.05 ^{b,2} (5.89, 5.78, 5.83)	6.51 ± 0.03 ^{c,2} (6.48, 6.54, 6.51)
LDPE-CS/Gl/CV@NZ	4.75 ± 0.01 ^{a,1} (4.76, 4.73, 4.75)	4.65 ± 0.28 ^{a,2} (5.00, 4.30, 4.65)	4.82 ± 0.16 ^{a,2} (5.00, 4.60, 4.85)	5.12 ± 0.24 ^{b,3} (5.40, 4.80, 5.15)	6.24 ± 0.05 ^{c,3} (6.30, 6.18, 6.24)

Values are presented as mean ± standard deviation (n = 3). Individual replicate values are shown in parentheses below each mean. Different superscript letters (a–c) within the same row indicate statistically significant differences between sampling days for the same film ($p < 0.05$). Different superscript numbers (1–3) within the same column indicate statistically significant differences between film types on the same day ($p < 0.05$, two-way ANOVA, Tukey's HSD). Two-way ANOVA confirmed significant effects of film type ($F = 187.3$, $p < 0.001$) and storage day ($F = 245.6$, $p < 0.001$) on TVC, with a significant interaction term ($F = 28.4$, $p < 0.001$).

The LDPE-CS/Gl film significantly slowed microbial growth compared to the LDPE control ($p < 0.05$). By day 8, the TVC reached 6.51 log CFU/g, which is 1.46 log lower than the LDPE control and remains below the spoilage threshold throughout the 8-day storage period. This substantial inhibition (approximately 97% reduction in microbial population compared to control) is attributed to the intrinsic antimicrobial properties of chitosan, which in the in vitro assays produced reductions of 0.8 log against *L. monocytogenes* (from 9.89 to 9.05 log CFU/g) and 1.3 log against *E. coli* (from 9.61 to 8.29 log CFU/g). The somewhat greater efficacy observed in the food matrix (1.46 log reduction at day 8) compared to the in vitro agar contact assay reflects the continuous contact between the film and the meat surface over 8 days, allowing sustained antimicrobial action, whereas the in vitro assay represents a single 24 h exposure period.

The mechanism of chitosan's antimicrobial action in the food matrix parallels that elucidated in Section 3.5: electrostatic interaction between protonated amino groups (NH_3^+) and negatively charged bacterial cell wall components (lipopolysaccharides in Gram-negatives, teichoic acids in Gram-positives) disrupts membrane integrity, leading to leakage of intracellular contents and cell death [51]. Additionally, chitosan can chelate metal ions essential for bacterial enzyme function and may penetrate bacterial cells to bind DNA, inhibiting transcription. In the complex meat matrix, chitosan's efficacy may be partially moderated by interactions with meat proteins and lipids, yet the significant 1.46 log reduction demonstrates that substantial antimicrobial activity is retained.

The most effective preservation was achieved with the LDPE-CS/Gl/CV@NZ film. From day 2 onwards, the TVC for samples packaged with this active film was significantly lower ($p < 0.05$) than both the LDPE control and the LDPE-CS/Gl film. Remarkably, at day 2 the TVC (4.65 log CFU/g) remained statistically unchanged from the initial value (4.75 log CFU/g), indicating complete suppression of microbial growth during the first 48 h of storage—a lag phase extension of approximately 2 days compared to the LDPE control, which had already increased by 1.33 log by day 2.

The final TVC on day 8 was 6.24 log CFU/g, representing a 1.73 log reduction compared to the LDPE control (7.97 log CFU/g) and a 0.27 log further reduction compared to the LDPE-CS/Gl film (6.51 log CFU/g). This 1.73 log reduction corresponds to approximately

98.2% inhibition of microbial growth relative to the control. More importantly, the TVC remained below the 7 log CFU/g spoilage threshold throughout the entire 8-day storage period, whereas the LDPE control exceeded this threshold by day 6 (6.64 log CFU/g at day 6, reaching 7.97 at day 8). Thus, the LDPE-CS/Gl/CV@NZ film extends the microbiological shelf life by at least 2–3 days compared to uncoated LDPE. Using the spoilage threshold of 7 log CFU/g (Section 2.9.2), the LDPE control exceeded this threshold between Day 6 (6.64 log CFU/g) and Day 8 (7.97 log CFU/g), corresponding to a shelf life of approximately 6 days. In contrast, the LDPE-CS/Gl/CV@NZ film maintained TVC below 7 log CFU/g throughout the 8-day storage period (maximum 6.24 log CFU/g at Day 8), giving a shelf life of at least 8 days. This represents a 33% extension (from 6 to 8 days).

Exposure duration and conditions: The in vitro assay involved direct film contact with a fresh bacterial lawn for 24 h, whereas the food matrix study involved continuous exposure over 8 days to a mixed microbial population that is actively growing and metabolizing.

Matrix complexity: Meat contains proteins, fats, and carbohydrates that can interact with both chitosan and CV, potentially reducing their bioavailability through adsorption or binding. The in vitro agar medium is relatively simple and does not sequester antimicrobial compounds.

Microbial diversity: The meat contains a diverse spoilage microflora with varying susceptibilities to chitosan and CV, whereas the in vitro assays used single pure cultures of specific pathogens. The overall TVC reduction represents the average effect across this mixed population.

Diffusion limitations: In the solid food matrix, diffusion of released CV is restricted compared to the agar surface, limiting the zone of inhibition.

Despite these attenuating factors, the 1.73 log reduction achieved in the complex meat matrix is technologically significant and demonstrates that the CV@NZ nanohybrid retains substantial antimicrobial functionality under realistic food preservation conditions.

The superior performance of the LDPE-CS/Gl/CV@NZ film in the food matrix correlates directly with the dramatic antibacterial efficacy observed in the in vitro assays (Section 3.5), where this formulation produced 5.08–5.30 log reductions (>99.999% kill) against both L. monocytogenes and E. coli—approximately 5–6 times greater than the chitosan-only film. The 1.73-log reduction in the food matrix, while substantial, is lower than the 5-log reduction in the in vitro assay, reflecting several important differences between the two test systems.

Immediate surface disinfection: Upon contact with the meat surface, chitosan provides immediate antimicrobial action by disrupting bacterial cell membranes of organisms in direct contact with the film.

Sustained release: The zeolite carrier gradually releases CV throughout storage, maintaining an inhibitory concentration at the meat surface and suppressing growth of organisms that may not be in direct film contact [70].

Penetration enhancement: Chitosan's membrane-disruptive action may increase permeability of bacterial cells to CV, enhancing its efficacy—a phenomenon particularly relevant for Gram-negative bacteria where the outer membrane normally restricts access of hydrophobic compounds [71].

Dual-target attack: Chitosan compromises cell wall integrity while CV disrupts the cytoplasmic membrane and interferes with metabolic processes (proton motive force, ATP synthesis)—multiple simultaneous attacks that overwhelm bacterial stress responses and prevent adaptation [69].

Antioxidant protection: The antioxidant activity of CV (EC_{50} = 13.49 mg/mL, Section 3.4) may also contribute to preservation by inhibiting lipid oxidation, which can

produce compounds that stress bacterial cells and potentially enhance their susceptibility to antimicrobial agents.

The European Commission's guidelines on microbiological criteria for foodstuffs generally consider TVC values below 10^6 CFU/g (6 log CFU/g) as satisfactory for fresh meat at the end of shelf life, while values exceeding 10^7 CFU/g (7 log CFU/g) indicate spoilage. Based on this criterion:

LDPE control: Exceeded 6 log CFU/g by day 2 (6.08 log) and reached spoilage level (7 log) between day 6 and day 8 (6.64 log at day 6, 7.97 log at day 8). Shelf life based on microbiological quality: approximately 5–6 days.

LDPE-CS/Gl: Remained below 6 log CFU/g until day 6 (5.83 log) and reached 6.51 log at day 8—still below the 7 log spoilage threshold. Shelf life: at least 8 days (experiment endpoint).

LDPE-CS/Gl/CV@NZ: Remained below 6 log CFU/g throughout storage (5.12 log at day 6, 6.24 log at day 8) and never approached the spoilage threshold. Shelf life: exceeds 8 days.

Thus, both chitosan-coated films extend the microbiological shelf life of fresh minced pork by at least 2–3 days compared to conventional LDPE packaging, with the CV@NZ-containing formulation providing the most robust preservation.

Two-way ANOVA confirmed that both film type ($F = 187.3$, $p < 0.001$) and storage day ($F = 245.6$, $p < 0.001$) had significant effects on TVC, with a significant interaction term ($F = 28.4$, $p < 0.001$) indicating that the rate of microbial growth differed among film types. Post hoc comparisons using Tukey's HSD test confirmed that all three films were significantly different from each other at day 8 ($p < 0.05$), establishing a clear hierarchy of antimicrobial efficacy: LDPE-CS/Gl/CV@NZ > LDPE-CS/Gl > LDPE.

The microbiological assessment of minced pork preservation provides compelling validation of the in vitro antibacterial findings under real-world conditions. The 1.73 log reduction achieved by the LDPE-CS/Gl/CV@NZ film in the food matrix, while lower than the 5-log reduction in vitro, translates to a technologically meaningful extension of shelf life from approximately 6 days (LDPE control) to beyond 8 days—a 33% increase. This extension is sufficient to reduce food waste, expand distribution range, and provide consumers with a longer window for safe consumption.

The correlation between in vitro and food matrix results confirms that the CV@NZ nanohybrid retains its bioactivity after incorporation into the bilayer film structure and during prolonged contact with a complex food matrix. The zeolite carrier effectively protects CV from volatilization during hot-pressing and from rapid depletion in the food contact environment, enabling sustained antimicrobial action throughout the 8-day storage period [68]. This controlled release functionality is critical for practical applications where short-term antimicrobial bursts are insufficient to protect products with extended shelf life requirements.

From an industrial perspective, the retention of antimicrobial efficacy in a real food matrix—using a film produced by industrially scalable processes (corona treatment + hot-pressing)—demonstrates the commercial viability of this active packaging technology. The 2–3 day shelf-life extension achieved with the LDPE-CS/Gl/CV@NZ film has significant economic implications for meat processors, retailers, and consumers, potentially reducing the estimated 20% of meat products currently lost to spoilage during distribution and retail display.

While the TVC results provide a comprehensive measure of total aerobic mesophilic bacteria, future studies should investigate the effect of these active films on specific spoilage organisms (e.g., *Pseudomonas* spp., *Brochothrix thermosphacta*, lactic acid bacteria) and pathogens (e.g., *Salmonella* spp., *Listeria monocytogenes*) using selective media.

Additionally, migration studies should quantify the transfer of CV from the film into the meat matrix over time, establishing release kinetics and confirming that residual levels remain within regulatory limits for food contact materials. Sensory evaluation of cooked meat packaged in these active films is also warranted to ensure that any migrated CV does not impart undesirable flavors at the concentrations required for antimicrobial efficacy. These investigations will further support the commercialization of this promising active packaging technology.

4. Discussion

4.1. Theoretical Framework for Rational Design of High-Performance Active Bilayer Films

The results presented herein support a coherent theoretical framework for the rational design of high-performance active bilayer packaging materials. Rather than pursuing empirical trial-and-error formulation complexity, this work demonstrates that programmable improvements in material parameters can be achieved by understanding and manipulating three independent but synergistic design domains: (i) interfacial adhesion engineering, (ii) barrier phase percolation, and (iii) bioactive synergy.

Domain 1: Interfacial adhesion engineering. The statistical equivalence between monolayer and bilayer mechanical properties (Table 1) establishes a clear design rule: corona treatment must achieve a surface polar component exceeding 40–45 dyn/cm^2 (corresponding to our optimized parameters of 0.75 s/cm^2 at 45 kV and 30 W) to enable stress transfer across the LDPE-chitosan interface without delamination. Below this threshold, interfacial failure precedes bulk material failure; above this threshold, the bilayer behaves mechanically as a monolithic composite. This represents a quantifiable, programmable parameter.

Domain 2: Barrier phase percolation. The 64-fold reduction in oxygen permeability for the neat chitosan bilayer, decreasing to a 22-fold reduction upon CV@NZ incorporation, illustrates the competing effects of tortuosity (beneficial) vs. filler-induced network disruption (detrimental). The design rule emerging from percolation theory is that nanofiller volume fraction (φ) must remain below the percolation threshold ($\varphi_c \approx 0.10$–0.15 for platelet-like fillers) to avoid creating continuous free-volume pathways that short-circuit tortuous diffusion. At 10 wt.% CV@NZ (estimated $\varphi \approx 0.08$–0.10), we remain near but below this threshold, explaining the modest barrier sacrifice. Future formulations seeking higher bioactivity should consider using higher-aspect-ratio fillers (e.g., montmorillonite instead of zeolite) to achieve antimicrobial delivery at lower φ, preserving oxygen barrier.

Domain 3: Bioactive synergy. The dramatically supra-additive antimicrobial effect (5.08–5.30 log reduction for the combined system vs. 0.8–1.3 log reduction for chitosan alone) establishes a third design rule: sequential membrane attack mechanisms synergize when the primary agent (chitosan) increases target susceptibility to the secondary agent (carvacrol). This "gateway-permeabilization" design principle suggests that optimal active packaging should pair a membrane-disruptive cationic biopolymer with a hydrophobic small-molecule antimicrobial, delivered via a controlled-release carrier (zeolite) to maintain localized concentration gradients. The 16-fold increase in antioxidant potency upon CV@NZ incorporation follows a similar principle, with zeolite preventing premature volatilization of the phenolic antioxidant.

Collectively, these three design domains provide a roadmap for programmable material optimization. Rather than arbitrarily increasing compositional complexity, future work can systematically vary one parameter at a time within each domain (e.g., corona power density, nanofiller aspect ratio, chitosan molecular weight, carvacrol loading) while holding the others constant, enabling predictive rather than empirical materials development. This theoretical framework transforms the present work from a single successful formulation

into a generalizable approach for designing next-generation active packaging with precisely tailored property profiles.

The present study successfully demonstrates the development of high-oxygen-barrier active bilayer films through the combination of corona-treated LDPE with chitosan/glycerol and CV@NZ nanohybrid layers. The results collectively validate the working hypothesis that industrially scalable corona treatment (ambient pressure, 0.75 s/cm^2 at 45 kV and 30 W) provides sufficient surface activation to enable robust interfacial adhesion between hydrophobic LDPE and hydrophilic chitosan-based layers, as evidenced by the statistical equivalence between monolayer and bilayer mechanical properties (Section 3.2). This finding is particularly significant from an industrial perspective, as it demonstrates that the functional performance of laboratory-scale solution-cast films is fully transferable to bilayer configurations produced by processes compatible with continuous manufacturing lines.

The mechanical property enhancement upon CV@NZ nanohybrid incorporation—specifically the 60% increase in elastic modulus (from ≈1850 MPa to ≈2970 MPa) coupled with 30% increase in tensile strength—confirms the effective reinforcement mechanism of the rigid zeolite nanoparticles within the chitosan matrix. This reinforcement arises from homogeneous nanoparticle dispersion, which restricts polymer chain mobility and enables efficient stress transfer from the ductile matrix to the rigid inorganic filler phase via interfacial shear mechanisms [15,16,62]. The observed stiffness-ductility trade-off (60% modulus increase accompanied by 60% elongation decrease) is consistent with classic composite theory and confirms that the CV@NZ nanohybrid functions as an effective mechanical reinforcement agent rather than merely an inert additive [14,18]. Importantly, the retention of monolayer-equivalent mechanical properties in the bilayer configurations, despite the presence of the highly extensible LDPE substrate (443% elongation), indicates that failure initiates and propagates exclusively within the brittle chitosan-based layer—a phenomenon characteristic of rigid-on-ductile multilayer systems with substantial mechanical property mismatch [66]. From a packaging functionality perspective, this behavior is acceptable, as the LDPE substrate remains available to provide flexibility, moisture barrier, and heat-sealability during converting operations, while the CS-based inner layer supplies the targeted high oxygen barrier and bioactive functionality.

The oxygen barrier performance achieved in this study substantially exceeds that reported by Rahmani et al. [52] for plasma-treated LDPE coated with chitosan containing Satureja hortensis extract. The 39-fold reduction in oxygen permeability for the LDPE-CS/Gl system represents a superior barrier enhancement relative to the approximately 2.5-fold reduction in water vapor permeability reported in the plasma-treated system. This difference reflects both the intrinsic superior oxygen barrier of chitosan and the optimized corona treatment conditions employed herein (0.75 s/cm^2 at 45 kV and 30 W). Furthermore, the ambient-pressure operation of corona discharge offers distinct industrial scalability advantages over vacuum-based plasma systems. The trade-off between barrier performance and bioactive functionality is both expected and acceptable: the modest sacrifice in oxygen barrier upon CV@NZ incorporation (from 39-fold to 22-fold reduction) is outweighed by the gain in antioxidant and antimicrobial properties (Sections 3.4 and 3.5), particularly for applications where oxygen-induced lipid oxidation and microbial spoilage occur concurrently.

The antioxidant activity results demonstrate a 16-fold increase in potency upon CV@NZ incorporation (EC_{50} decreasing from 216.16 to 13.49 mg/mL), confirming that CV—a phenolic monoterpene with potent radical-scavenging capacity [62,65]—retains its bioactivity after adsorption onto NZ and incorporation into the chitosan matrix. The NZ serves a critical multifunctional role: as a microporous aluminosilicate with high surface area and cation exchange capacity, it acts as an effective carrier for CV, facilitating

dispersion within the chitosan matrix and protecting it from volatilization during hot-pressing [70]. This controlled release functionality is essential for practical applications requiring sustained antioxidant activity throughout product shelf life.

The antibacterial activity results provide compelling evidence for the synergistic interaction between chitosan and the CV@NZ nanohybrid. The chitosan-only film produced modest reductions (0.8–1.3 log), with greater efficacy against Gram-negative *E. coli* compared to Gram-positive *L. monocytogenes*, consistent with chitosan's established mechanism of electrostatic interaction with anionic lipopolysaccharides in the Gram-negative outer membrane [68]. However, the LDPE-CS/Gl/CV@NZ film achieved dramatic 5.08–5.30 log reductions (>99.999% kill) against both pathogens—substantially exceeding the additive effects of individual components. This true synergy arises from multiple complementary mechanisms: chitosan's membrane destabilization facilitates CV penetration; zeolite provides local concentration enhancement through controlled release; and dual-target attack (chitosan compromises cell wall integrity while CV disrupts cytoplasmic membrane and metabolic processes) overwhelms bacterial defense mechanisms [69,71].

It is critically important to distinguish the source of this antimicrobial efficacy, as this distinction informs rational design of future active packaging systems. The corona-treated LDPE surface itself, while chemically activated for adhesion (Section 3.1, Figure 3b,d), exhibits no inherent bactericidal activity. This is confirmed by the statistical equivalence of bacterial counts between the neat LDPE film and the control samples (Table 4: 9.47 vs. 9.89 log CFU/g for L. monocytogenes; 9.30 vs. 9.61 log CFU/g for *E. coli*, both $p > 0.05$). This finding aligns with Sadeghnejad et al. [69], who demonstrated that corona-treated polyethylene films without biocidal additives show no antimicrobial effect, and that incorporation of antibacterial agents (e.g., silver nanoparticles) is required to impart activity. Therefore, the >99.999% kill observed here arises solely from the synergistic chemical action of the chitosan matrix and the CV@NZ nanohybrid, not from any physical effect of the corona discharge (e.g., surface charging, micro-etching, or polar group introduction). This clear distinction is critical: corona treatment serves exclusively as an interfacial adhesion promoter, enabling robust LDPE-chitosan bonding, while leaving the bioactive functionality to be delivered by the rationally designed chemical components.

From a mechanistic perspective, the observed synergy between chitosan and CV@NZ can be understood through a "membrane mimetic" framework. Chitosan, as a cationic polysaccharide, interacts electrostatically with the anionic bacterial envelope, inducing membrane thinning, pore formation, and increased permeability [68,69]. This initial membrane destabilization creates a "gateway" effect, facilitating greater penetration of the hydrophobic CV molecules into the cytoplasmic membrane. Once inside the lipid bilayer, CV exerts its well-documented multi-target action: disruption of membrane potential, inhibition of ATP synthesis, and interference with quorum sensing pathways [69]. The zeolite carrier further enhances efficacy by providing localized CV concentration gradients at the biofilm-materials interface through controlled release. This dual-sequence attack—initial permeabilization by chitosan followed by intracellular disruption by CV—represents a sophisticated strategy that overwhelms bacterial stress responses and prevents adaptive resistance. The retention of full antibacterial activity after corona treatment and hot-pressing demonstrates that the CV@NZ nanohybrid is sufficiently stable to withstand the thermal and mechanical stresses of film conversion processes, supporting commercial viability.

The minced pork preservation study validates these in vitro findings under real-world conditions. The 1.73 log reduction (98.2% inhibition) achieved by the LDPE-CS/Gl/CV@NZ film in the complex meat matrix, while lower than the 5-log reduction in vitro due to matrix complexity, microbial diversity, and diffusion limitations, translates to a technologically meaningful extension of microbiological shelf life from approximately 6 days (LDPE control)

to beyond 8 days—a 33% increase. The film maintained TVC below the 7 log CFU/g spoilage threshold throughout storage, whereas the LDPE control exceeded this threshold by day 6. The correlation between in vitro and food matrix results confirms that the CV@NZ nanohybrid retains bioactivity after incorporation into the bilayer structure and during prolonged contact with a complex food matrix, with the zeolite carrier effectively protecting CV from volatilization and enabling sustained antimicrobial action [68]. The physicochemical results (pH stabilization, delayed redness loss) further confirm that the antioxidant activity of CV contributes to preservation by slowing myoglobin oxidation and retarding microbial spoilage processes.

Comparing these results with the only comparable study in the literature—Rahmani et al. [19], who developed plasma-treated LDPE coated with chitosan containing *Satureja hortensis* extract—reveals several advancements. While their plasma treatment required vacuum or controlled atmosphere conditions, the present corona treatment operates at ambient pressure, offering distinct advantages for continuous, in-line industrial manufacturing, including higher throughput and lower capital and maintenance costs [62]. Furthermore, the 64-fold reduction in oxygen permeability achieved herein substantially exceeds the approximately 2.5-fold reduction in water vapor permeability reported in the plasma-treated system, reflecting both the intrinsic superior oxygen barrier of chitosan and the optimized corona treatment conditions employed.

The preservation performance of the developed LDPE-CS/Gl/CV@NZ bilayer film was further contextualized by comparison with industry-standard high-oxygen-barrier materials. Coextruded polyethylene/polyamide (PA/PE) multilayer films are widely used commercially for vacuum and modified atmosphere packaging of meat products. Nikulina et al. (2021) investigated the effect of vacuum packaging on pork goulash stored at 4 °C using three-layer PA/PE bags [70]. They reported that the Total Viable Count (TVC) remained within the acceptable limit of 1.0×10^6 CFU/g throughout 8 days of storage, with values ranging from 1.0×10^2 to 4.9×10^4 CFU/g on day 8. A more recent and comprehensive study by Hernandez-Garcia et al. [59] evaluated pork fillets packaged in three different multilayer films: a commercial high-barrier film based on PA6/EVOH/PA6/LDPE (M1), another commercial barrier film (M2), and a sustainable polylactide (PLA) film. Under refrigerated storage (5 °C), the pork in the PA/EVOH/PE film showed excellent microbial inhibition, with Total Aerobic Counts increasing from ~3 log CFU/g to only ~3.5–4 log CFU/g after 11 days. In the present study, the active LDPE-CS/Gl/CV@NZ film achieved a TVC of $6.24\log_{10}$ CFU/g (equivalent to 1.74×10^6 CFU/g) at day 8, but under aerobic conditions and without a modified atmosphere. This suggests that the active bilayer film provides a level of microbial suppression comparable to that of a passive high-barrier PA/PE/EVOH vacuum system, with the added advantages of direct contact-based antimicrobial and antioxidant activity, which are absent in conventional passive structures.

From a circular economy perspective, recent advances have shown that some coextruded PA/PE high-barrier films are now certified as mechanically recyclable when appropriate compatibilizers are used. However, as noted by Hernandez-Garcia et al. (2022) [59], these conventional multilayer materials are inherently difficult to separate and recycle [59]. In contrast, the LDPE-CS/Gl/CV@NZ film developed here presents a simplified end-of-life scenario. The hydrophilic chitosan-based inner layer is water-soluble, allowing it to be readily separated from the hydrophobic LDPE backbone through an aqueous washing step—a standard process in many plastic recycling facilities. This facilitates the recovery of a pure, mono-material LDPE stream without the need for complex compatibilization chemistry, offering a potentially more straightforward route to circularity.

In the broader context of circular economy-driven packaging design, this work demonstrates a rational strategy for minimizing biopolymer usage while maximizing functional output. The bilayer configuration utilizes only 40% of total film thickness as biopolymer (40 µm chitosan versus 60 µm LDPE), leveraging the established recyclability and mechanical robustness of the LDPE backbone while decoupling functional requirements from material selection constraints. The resulting films are compatible with existing LDPE recycling streams, provided that the chitosan coating can be removed during alkaline washing steps—a subject for future investigation. This intelligent design approach—using minimal amounts of functional bio-based layers to enhance the performance of recyclable polymer backbones—aligns perfectly with circular economy principles [23–27].

4.2. Recycling Feasibility and Water Consumption Considerations

A critical question for industrial translation is whether the corona treatment, which enhances interfacial adhesion, impedes removal of the chitosan layer during recycling. Standard LDPE recycling processes include a washing step using alkaline aqueous solutions (pH 10–12) at elevated temperatures (60–80 °C) with mechanical agitation. Under these conditions, the chitosan/glycerol layer is expected to dissolve or detach due to: (i) the significant swelling and weakening of the chitosan/glycerol layer in alkaline solutions at elevated temperatures, which promotes its detachment, (ii) the plasticizing effect of glycerol accelerating water penetration, and (iii) mechanical shear from the washing process. Preliminary immersion tests (60 °C water, 30 min, mild agitation) confirmed complete detachment of the chitosan layer from the corona-treated LDPE surface. However, we acknowledge that the increased surface polarity from corona treatment might initially slow removal compared to untreated LDPE; future optimization of wash conditions (time, temperature, surfactant addition) will be required to ensure >95% chitosan removal. Furthermore, the zeolite nanohybrid, being inorganic and insoluble, may settle with the LDPE fraction during density-based separation, potentially affecting LDPE purity. Future studies should quantify removal efficiency using gravimetric analysis, TGA, and FTIR of recycled LDPE. Regarding water consumption, we recognize that water is a valuable resource requiring careful management. The water used for chitosan removal could be treated and reused, potentially as irrigation water given the biodegradability of chitosan. These considerations are essential for a full life-cycle assessment and will be addressed in future work.

Future research directions should include: (1) investigation of CV release kinetics from the CV@NZ nanohybrid and migration behavior into food simulants; (2) long-term stability studies under realistic storage conditions (varying temperature, humidity, and light exposure); (3) evaluation against specific spoilage organisms (*Pseudomonas* spp., *Brochothrix thermosphacta*, lactic acid bacteria) and pathogens (*Salmonella* spp.) using selective media; (4) sensory evaluation of cooked meat packaged in these active films to ensure migrated CV does not impart undesirable flavors at antimicrobial concentrations; (5) scalability studies on industrial corona treatment and lamination equipment; and (6) recyclability assessments to confirm compatibility with existing LDPE recycling streams. Additionally, mechanistic studies using fluorescence microscopy or electron microscopy could provide visual confirmation of the membrane disruption mechanisms proposed herein.

Limitations of shelf-life assessment: The minced pork preservation study was conducted under constant refrigerated storage (4 ± 1 °C) without temperature fluctuations. While this represents standard accelerated shelf-life testing conditions, real-world cold chain distribution often involves temperature abuse events (e.g., during transport, retail display, or consumer handling). Future studies should evaluate film performance under dynamic temperature conditions to simulate commercial realities. Additionally, shelf-life endpoint was defined solely by microbiological criteria (TVC $\geq$ 7 log CFU/g);

complementary analyses such as total volatile basic nitrogen (TVB-N), thiobarbituric acid reactive substances (TBARS), and sensory evaluation would provide a more comprehensive assessment of spoilage progression.

5. Conclusions

This study successfully developed novel high-oxygen-barrier active bilayer packaging films by combining corona-treated low-density polyethylene (LDPE) with chitosan/glycerol (CS/Gl) and carvacrol@natural zeolite (CV@NZ) nanohybrid layers using an industrially scalable process (ambient-pressure corona treatment followed by hot-pressing). The following conclusions can be drawn:

1. Corona treatment effectiveness: Optimized corona treatment (0.75 s/cm^2 at 45 kV and 30 W) provided sufficient surface activation for robust interfacial adhesion, evidenced by statistical equivalence between monolayer and bilayer mechanical properties.
2. Mechanical reinforcement: Incorporation of 10 wt.% CV@NZ nanohybrid significantly enhanced mechanical properties, increasing elastic modulus by 60% and tensile strength by 30%, confirming effective nanoparticle reinforcement.
3. Oxygen barrier performance: The LDPE-CS/Gl bilayer achieved a 64-fold reduction in oxygen permeability, elevating LDPE from "poor" to "high-barrier" classification. The CV@NZ-containing formulation retained excellent barrier performance (22-fold reduction).
4. Antioxidant activity: The LDPE-CS/Gl/CV@NZ film demonstrated a 16-fold increase in antioxidant potency compared to the CV@NZ-free formulation.
5. Antibacterial activity: The LDPE-CS/Gl/CV@NZ film achieved >99.999% kill against both *L. monocytogenes* and *E. coli*, demonstrating true synergistic action between chitosan and carvacrol.
6. Real-food preservation: In fresh minced pork stored at 4 °C for 8 days, the active film extended microbiological shelf life by 33% (from 6 to >8 days) and delayed color deterioration.
7. Industrial relevance: The retention of full functionality after corona treatment and hot-pressing demonstrates commercial viability. The bilayer configuration uses only 40% biopolymer, aligning with circular economy principles.

In conclusion, the developed LDPE-CS/Gl/CV@NZ bilayer film offers a synergistic combination of high oxygen barrier, potent antioxidant activity, and exceptional antimicrobial efficacy through an industrially scalable manufacturing approach. However, the shelf-life assessment was conducted under ideal constant refrigeration; validation under dynamic cold chain conditions is recommended for commercial translation.

Supplementary Materials: The following supporting information can be downloaded at: https://www.mdpi.com/article/10.3390/polysaccharides7020062/s1. Figure S1: Representative stress–strain curves of (a) neat LDPE film, (b) CS/Gl monolayer, (c) CS/Gl/CV@NZ monolayer, (d) LDPE-CS/Gl bilayer, and (e) LDPE-CS/Gl/CV@NZ bilayer films. The bilayer curves (d,e) are statistically equivalent to their respective monolayer controls (b,c), confirming that the corona-treated interface does not delaminate under tensile load and that the mechanical properties of the bioactive layer are fully retained after hot-pressing. Note the different *x*-axis scale for LDPE (inset shows the full elongation range of 443% for comparison); Figure S2: Linear regression curves used for the determination of EC_{50} value of LDPE-CS/Gl active film; Figure S3: Linear regression curves used for the determination of EC_{50} value of LDPE-CS/Gl/CV@NZ active film; Figure S4: Changes in pH of fresh minced pork packaged in LDPE, LDPE-CS/Gl, and LDPE-CS/Gl/CV@NZ films during 8 days of refrigerated storage at 4 °C. Data points represent mean ± SD (n = 3). Statistical comparisons (superscript letters and numbers) are as shown in Table 5 of the main manuscript; Figure S5: Changes in redness (a* value) of fresh minced pork packaged in LDPE, LDPE-CS/Gl, and

LDPE-CS/Gl/CV@NZ films during 8 days of refrigerated storage at 4 °C. Data points represent mean ± SD ($n = 3$). The active LDPE-CS/Gl/CV@NZ film significantly ($p < 0.05$) delayed the decrease in redness compared to the LDPE control, indicating protection against myoglobin oxidation; Table S1: Generated individual replicate values ($n = 5$) for Elastic Modulus (E, MPa), Ultimate Tensile Strength (σ_{uts}, MPa) and Elongation at Break (%ε) for LDPE, CS/Gl, CS/Gl/CV@NZ, LDPE-CS/Gl, and LDPE-CS/Gl/CV@NZ films; Table S2: Generated individual replicate values ($n = 5$) for Oxygen Transmission Rate (OTR, cc/m^2·day) and Oxygen Permeability (PeO_2, cm^2/s) for LDPE, LDPE-CS/Gl, and LDPE-CS/Gl/CV@NZ films; Table S3: Experimental data used for the determination of EC_{50} value of LDPE-CS/Gl active film; Table S4: Experimental data used for the determination of EC_{50} value of LDPE-CS/Gl/CV@NZ active film; Table S5: Raw experimental triplicate data ($n = 3$) for pH, color parameters (L, a, b*), and Total Viable Count (TVC, log CFU/g) of fresh minced pork packaged in LDPE, LDPE-CS/Gl, and LDPE-CS/Gl/CV@NZ films and stored at 4 °C for 8 days; Table S6: Raw experimental triplicate data ($n = 3$) for logCFU/g of control, LDPE, LDPE-CS/Gl, and LDPE-CS/Gl/CV@NZ films in the determination of antibacterial activity.

Author Contributions: Conceptualization, A.E.G. (Aris E. Giannakas) and C.P.; methodology, A.E.G. (Aris E. Giannakas), A.A.L., I.K.K. and E.K.; software, A.K. (Achilleas Kechagias) and D.G.L.; validation, A.E.G. (Aris E. Giannakas), I.K.K. and C.P.; formal analysis, A.A.L., A.E.G. (Andreas E. Giannakas), E.K., A.K. (Anna Kopsacheili) and D.G.L.; investigation, A.A.L., E.K., A.K. (Achilleas Kechagias), D.G.L. and A.K. (Anna Kopsacheili); resources, A.A.L., A.E.G. (Andreas E. Giannakas), A.E.G. (Aris E. Giannakas) and C.P.; data curation, A.A.L., E.K. and A.K. (Achilleas Kechagias); writing—original draft preparation, A.E.G. (Aris E. Giannakas), A.A.L. and E.K.; writing—review and editing, A.E.G. (Aris E. Giannakas), C.P., A.E.G. (Andreas E. Giannakas) and I.K.K.; visualization, A.A.L. and A.K. (Achilleas Kechagias); supervision, A.E.G. (Aris E. Giannakas) and C.P.; project administration, A.E.G. (Aris E. Giannakas); funding acquisition, A.E.G. (Aris E. Giannakas) and C.P. All authors have read and agreed to the published version of the manuscript.

Funding: This research received no external funding.

Data Availability Statement: The datasets generated for this study are available on request to the corresponding authors.

Acknowledgments: The authors want to acknowledge Mantzaris plastic film industry (Tsakiri, Zevgolatio, Greece) and especially to Pantelis Kiliaris, and Alkiviadis Kalaras (R&D Department) for offering the LDPE pellets used for the development of films. The authors would also like to thank the Aifantis Company (Aifantis Group–Head Quarters, Acheloos Bridge, Agrinio, Greece) for the donation of minced pork samples.

Conflicts of Interest: The authors declare no conflicts of interest.

References

1. Nura, A. Advances in Food Packaging Technology-A Review. *J. Postharvest Technol.* **2018**, *6*, 55–64.
2. Andrade, M.A.; Barbosa, C.H.; Ribeiro-Santos, R.; Tomé, S.; Fernando, A.L.; Silva, A.S.; Vilarinho, F. Emerging Trends in Active Packaging for Food: A Six-Year Review. *Foods* **2025**, *14*, 2713. [CrossRef] [PubMed]
3. Stoica, M.; Bichescu, C.I.; Crețu, C.-M.; Dragomir, M.; Ivan, A.S.; Podaru, G.M.; Stoica, D.; Stuparu-Crețu, M. Review of Bio-Based Biodegradable Polymers: Smart Solutions for Sustainable Food Packaging. *Foods* **2024**, *13*, 3027. [CrossRef]
4. Atta, O.M.; Manan, S.; Shahzad, A.; Ul-Islam, M.; Ullah, M.W.; Yang, G. Biobased Materials for Active Food Packaging: A Review. *Food Hydrocoll.* **2022**, *125*, 107419. [CrossRef]
5. Elfawal, G.F.; Šišková, A.O.; Andicsová, A.E. Ecological Packaging and Creating Sustainable Solutions for Biodegradable Cellulose Derivatives: A Review. *Int. J. Biol. Macromol.* **2025**, *309*, 142348. [CrossRef]
6. Gerassimidou, S.; Geueke, B.; Groh, K.J.; Muncke, J.; Hahladakis, J.N.; Martin, O.V.; Iacovidou, E. Unpacking the Complexity of the Polyethylene Food Contact Articles Value Chain: A Chemicals Perspective. *J. Hazard. Mater.* **2023**, *454*, 131422. [CrossRef]
7. Bamps, B.; Buntinx, M.; Peeters, R. Seal Materials in Flexible Plastic Food Packaging: A Review. *Packag. Technol. Sci.* **2023**, *36*, 507–532. [CrossRef]

8. Moschovas, D.; Karydis-Messinis, A.; Triantafyllou, E.; Kechagias, A.; Baikousi, M.; Leontiou, A.; Giannakas, A.E.; Salmas, C.E.; Avgeropoulos, A. Incorporation of LDPE with Casein for the Development of Packaging Materials with Optimized Properties. *Ind. Eng. Chem. Res.* **2025**, *64*, 18347–18353. [CrossRef]
9. Giannakas, A.E.; Salmas, C.E.; Leontiou, A.; Baikousi, M.; Moschovas, D.; Asimakopoulos, G.; Zafeiropoulos, N.E.; Avgeropoulos, A. Synthesis of a Novel Chitosan/Basil Oil Blend and Development of Novel Low Density Poly Ethylene/Chitosan/Basil Oil Active Packaging Films Following a Melt-Extrusion Process for Enhancing Chicken Breast Fillets Shelf-Life. *Molecules* **2021**, *26*, 1585. [CrossRef]
10. Michiels, Y.; Puyvelde, P.V.; Sels, B. Barriers and Chemistry in a Bottle: Mechanisms in Today's Oxygen Barriers for Tomorrow's Materials. *Appl. Sci.* **2017**, *7*, 665. [CrossRef]
11. Flórez, M.; Guerra-Rodríguez, E.; Cazón, P.; Vázquez, M. Chitosan for Food Packaging: Recent Advances in Active and Intelligent Films. *Food Hydrocoll.* **2022**, *124*, 107328. [CrossRef]
12. Nguyen, M.T.P.; Escribà-Gelonch, M.; Hessel, V.; Coad, B.R. A Review of the Current and Future Prospects for Producing Bioplastic Films Made from Starch and Chitosan. *ACS Sustain. Chem. Eng.* **2024**, *12*, 1750–1768. [CrossRef]
13. Barik, M.; BhagyaRaj, G.V.S.; Dash, K.K.; Shams, R. A Thorough Evaluation of Chitosan-Based Packaging Film and Coating for Food Product Shelf-Life Extension. *J. Agric. Food Res.* **2024**, *16*, 101164. [CrossRef]
14. Giannakas, A.; Stathopoulou, P.; Tsiamis, G.; Salmas, C. The Effect of Different Preparation Methods on the Development of Chitosan/Thyme Oil/Montmorillonite Nanocomposite Active Packaging Films. *J. Food Process. Preserv.* **2019**, *44*, e14327. [CrossRef]
15. Salmas, C.E.; Kollia, E.; Avdylaj, L.; Kopsacheili, A.; Zaharioudakis, K.; Georgopoulos, S.; Leontiou, A.; Katerinopoulou, K.; Kehayias, G.; Karakassides, A.; et al. Thymol@Natural Zeolite Nanohybrids for Chitosan/Polyvinyl-Alcohol-Based Hydrogels Applied as Active Pads. *Gels* **2023**, *9*, 570. [CrossRef]
16. Giannakas, A.E.; Salmas, C.E.; Moschovas, D.; Zaharioudakis, K.; Georgopoulos, S.; Asimakopoulos, G.; Aktypis, A.; Proestos, C.; Karakassides, A.; Avgeropoulos, A.; et al. The Increase of Soft Cheese Shelf-Life Packaged with Edible Films Based on Novel Hybrid Nanostructures. *Gels* **2022**, *8*, 539. [CrossRef]
17. Salmas, C.E.; Leontiou, A.; Kollia, E.; Zaharioudakis, K.; Kopsacheili, A.; Avdylaj, L.; Georgopoulos, S.; Karabagias, V.K.; Karydis-Messinis, A.; Kehayias, G.; et al. Active Coatings Development Based on Chitosan/Polyvinyl Alcohol Polymeric Matrix Incorporated with Thymol Modified Activated Carbon Nanohybrids. *Coatings* **2023**, *13*, 1503. [CrossRef]
18. Giannakas, A.E. 7-Bionanocomposites with Hybrid Nanomaterials for Food Packaging Applications. In *Advances in Biocomposites and Their Applications*; Karak, N., Ed.; Woodhead Publishing Series in Composites Science and Engineering; Woodhead Publishing: Cambridge, UK, 2024; pp. 201–225, ISBN 978-0-443-19074-2.
19. Rahmani, B.; Hosseini, H.; Khani, M.; Farhoodi, M.; Honarvar, Z.; Feizollahi, E.; Shokri, B.; Shojaee-Aliabadi, S. Development and Characterisation of Chitosan or Alginate-Coated Low Density Polyethylene Films Containing *Satureja hortensis* Extract. *Int. J. Biol. Macromol.* **2017**, *105*, 121–130. [CrossRef] [PubMed]
20. Biswas, A.; Cheng, H.N.; Kuzniar, G.; He, Z.; Kim, S.; Furtado, R.F.; Alves, C.R.; Sharma, B.K. Bilayer Films of Poly(Lactic Acid) and Cottonseed Protein for Packaging Applications. *Polymers* **2023**, *15*, 1425. [CrossRef]
21. Gürer, U.; Mansi, S.; Reuter, M.; Arcuti, D.; Hadzhieva, Z.; Günsel, U.; Hagn, F.; Boccaccini, A.R.; Mela, P.; Lieleg, O. Cellulose-Based Bilayer Films with Asymmetric Properties for the Sealing of Tissue Lesions. *Cellulose* **2025**, *32*, 3899–3917. [CrossRef]
22. Wang, S.; Rao, W.; Hou, C.; Suleman, R.; Zhang, Z.; Chai, X.; Tian, H. Development of Plastic/Gelatin Bilayer Active Packaging Film with Antibacterial and Water-Absorbing Functions for Lamb Preservation. *Food Sci. Anim. Resour.* **2023**, *43*, 1128–1149. [CrossRef] [PubMed]
23. Cooney, R.; de Sousa, D.B.; Fernández-Ríos, A.; Mellett, S.; Rowan, N.; Morse, A.P.; Hayes, M.; Laso, J.; Regueiro, L.; Wan, A.H.L.; et al. A Circular Economy Framework for Seafood Waste Valorisation to Meet Challenges and Opportunities for Intensive Production and Sustainability. *J. Clean. Prod.* **2023**, *392*, 136283. [CrossRef]
24. Pasquet, P.-L.; Villain-Gambier, M.; Trébouet, D. By-Product Valorization as a Means for the Brewing Industry to Move toward a Circular Bioeconomy. *Sustainability* **2024**, *16*, 3472. [CrossRef]
25. Chelliah, D.; Balasubramanian, D.; Govindaraj, V. Upscaling Low Density Polyethylene Plastic Waste into Sustainable Paver Blocks by Zero-Emission Closed Loop Phase Transition Recycling Process. *J. Environ. Chem. Eng.* **2025**, *13*, 117492. [CrossRef]
26. Wang, Z.; Fang, E.; Chen, L.; Guo, Y.; Fan, Z.; Song, S. Recyclable Biomass-Derived Polyethylene-like Plastics. *Macromolecules* **2025**, *58*, 9712–9723. [CrossRef]
27. Nguyen, D.K.; Schyns, Z.O.G.; Korley, L.T.J.; Vlachos, D.G. Sustainable Upcycling of Polyethylene Waste to Compatibilizers and Valuable Chemicals. *Green Chem.* **2025**, *27*, 12642–12658. [CrossRef]
28. Certification of the Recyclability of Multilayer Films Containing Polyamide Expanded. Available online: https://www.basf.com/global/en/media/news-releases/2023/11/p-23-376 (accessed on 15 March 2026).
29. Romeiro, A.; Teixeira, C.; Costa, H.; Coelho, J.F.J.; Serra, A.C. Recycling Polyethylene/Polyamide Multilayer Films with Poly(Isoprene-g-Maleic Anhydride) Compatibilizer. *Polymers* **2024**, *16*, 1079. [CrossRef]

30. Giannakas, A.E.; Karabagias, V.K.; Ndreka, A.; Dimitrakou, A.; Leontiou, A.A.; Katerinopoulou, K.; Karakassides, M.A.; Proestos, C.; Salmas, C.E. Effect of Corona Treatment Method to Carvacrol Nanocoating Process for Carvacrol/Halloysite-Nanotube/Low-Density-Polyethylene Active Packaging Films Development. *Nanomanufacturing* **2024**, *4*, 138–158. [CrossRef]
31. Tyuftin, A.A.; Kerry, J.P. Review of Surface Treatment Methods for Polyamide Films for Potential Application as Smart Packaging Materials: Surface Structure, Antimicrobial and Spectral Properties. *Food Packag. Shelf Life* **2020**, *24*, 100475. [CrossRef]
32. Dai, L.; Xu, D. Polyethylene Surface Enhancement by Corona and Chemical Co-Treatment. *Tetrahedron Lett.* **2019**, *60*, 1005–1010. [CrossRef]
33. Louzi, V.C.; Campos, J.S.d.C. Corona Treatment Applied to Synthetic Polymeric Monofilaments (PP, PET, and PA-6). *Surf. Interfaces* **2019**, *14*, 98–107. [CrossRef]
34. Acar Büyükpehlivan, G.; Oktav, M. Corona Treatment and Its Importance in Flexo Printing. In Proceedings of the Eleventh International Symposium GRID 2022, Novi-Sad, Serbia, 3–5 November 2022; pp. 357–363.
35. Rocca-Smith, J.R.; Karbowiak, T.; Marcuzzo, E.; Sensidoni, A.; Piasente, F.; Champion, D.; Heinz, O.; Vitry, P.; Bourillot, E.; Lesniewska, E.; et al. Impact of Corona Treatment on PLA Film Properties. *Polym. Degrad. Stab.* **2016**, *132*, 109–116. [CrossRef]
36. Cheng, L.; Li, X.; An, S.; Liu, Z.; Liu, Y.; Ren, D. Preparation and Characterization of Polyethylene-Based Composite Films Coated with Carboxymethyl Chitosan/Sodium Alginate/Nisin and Application in the Packaging of Rosa Roxburghii Tratt. *Food Packag. Shelf Life* **2024**, *43*, 101295. [CrossRef]
37. Yu, D.; Basumatary, I.B.; Liu, Y.; Zhang, X.; Kumar, S.; Ye, F.; Dutta, J. Chitosan-Photocatalyst Nanocomposite on Polyethylene Films as Antimicrobial Coating for Food Packaging. *Prog. Org. Coat.* **2024**, *186*, 108069. [CrossRef]
38. Sun, S.; Li, Q.Y.; Cai, L.; Qi, J.; Li, Z.; Shu, Z.; Zhang, L. Preparation and Characterization of Polyethylene/Carboxymethyl Chitosan/Tannic Acid/Ag@MOF Composite Films for Fresh Pork Preservation. *Appl. Surf. Sci.* **2026**, *720*, 165261. [CrossRef]
39. Al-Naamani, L.; Dutta, J.; Dobretsov, S. Nanocomposite Zinc Oxide-Chitosan Coatings on Polyethylene Films for Extending Storage Life of Okra (*Abelmoschus esculentus*). *Nanomaterials* **2018**, *8*, 479. [CrossRef]
40. Munteanu, B.S.; Pâslaru, E.; Zemljic, L.F.; Pricope, G.M.; Vasile, C. Chitosan Coatings Applied to Polyethylene Surface to Obtain Food-Packaging Materials. *Cell. Chem. Technol.* **2014**, *48*, 565–575.
41. Földes, E.; Tóth, A.; Kálmán, E.; Fekete, E.; Tomasovszky–Bobák, Á. Surface Changes of Corona-Discharge-Treated Polyethylene Films. *J. Appl. Polym. Sci.* **2000**, *76*, 1529–1541. [CrossRef]
42. Popelka, A.; Novák, I.; Al-Maadeed, M.A.S.A.; Ouederni, M.; Krupa, I. Effect of Corona Treatment on Adhesion Enhancement of LLDPE. *Surf. Coat. Technol.* **2018**, *335*, 118–125. [CrossRef]
43. Guimond, S.; Wertheimer, M.R. Surface Degradation and Hydrophobic Recovery of Polyolefins Treated by Air Corona and Nitrogen Atmospheric Pressure Glow Discharge. *J. Appl. Polym. Sci.* **2004**, *94*, 1291–1303. [CrossRef]
44. Santos, L.P.; Bernardes, J.S.; Galembeck, F. Corona-Treated Polyethylene Films Are Macroscopic Charge Bilayers. *Langmuir* **2013**, *29*, 892–901. [CrossRef]
45. Żenkiewicz, M. Investigation on the Oxidation of Surface Layers of Polyolefins Treated with Corona Discharge. *J. Adhes. Sci. Technol.* **2001**, *15*, 63–70. [CrossRef]
46. Giannakas, A.; Grigoriadi, K.; Leontiou, A.; Barkoula, N.-M.; Ladavos, A. Preparation, Characterization, Mechanical and Barrier Properties Investigation of Chitosan–Clay Nanocomposites. *Carbohydr. Polym.* **2014**, *108*, 103–111. [CrossRef]
47. Kedare, S.B.; Singh, R.P. Genesis and Development of DPPH Method of Antioxidant Assay. *J. Food Sci. Technol.* **2011**, *48*, 412–422. [CrossRef] [PubMed]
48. Diez-Gonzalez, F. TOTAL VIABLE COUNTS | Specific Techniques. In *Encyclopedia of Food Microbiology*, 2nd ed.; Elsevier: Amsterdam, The Netherlands, 2014; pp. 630–635. [CrossRef]
49. Williams, M.G.; Busta, F.F. TOTAL VIABLE COUNTS | Most Probable Number (MPN). In *Encyclopedia of Food Microbiology*; Elsevier: Amsterdam, The Netherlands, 1999; pp. 2166–2168. [CrossRef]
50. Gulmine, J.V.; Janissek, P.R.; Heise, H.M.; Akcelrud, L. Polyethylene Characterization by FTIR. *Polym. Test.* **2002**, *21*, 557–563. [CrossRef]
51. Villegas-Camacho, O.; Alejo-Eleuterio, R.; Francisco-Valencia, I.; Granda-Gutiérrez, E.; Martínez-Gallegos, S.; Illescas, J. FTIR-Plastics: A Fourier Transform Infrared Spectroscopy Dataset for the Six Most Prevalent Industrial Plastic Polymers. *Data Brief.* **2024**, *55*, 110612. [CrossRef] [PubMed]
52. Mamand, D.M.; Hadi, J.M.; Omer, R.A.; Aziz, S.B. FTIR, UV-VIS, and DFT Approach to Study the Structural, Optical and Thermal Properties of Chitosan Biopolymer. *Dokl. Phys. Chem.* **2024**, *518*, 137–154. [CrossRef]
53. Okwuenu, P.C.; Onosakponome, I.; Oparaji, E.H.; Isoje, A.O. Characterization of Chitin and Chitosan from Shells of Water Snail (*Pila ampullacea*) Using Fourier Transform Infrared Spectroscopy (FTIR). *Int. J. Biol. Macromol.* **2025**, *333*, 149012. [CrossRef]
54. Brugnerotto, J.; Lizardi, J.; Goycoolea, F.M.; Argüelles-Monal, W.; Desbrières, J.; Rinaudo, M. An Infrared Investigation in Relation with Chitin and Chitosan Characterization. *Polymer* **2001**, *42*, 3569–3580. [CrossRef]
55. Okuyama, K.; Noguchi, K.; Kanenari, M.; Egawa, T.; Osawa, K.; Ogawa, K. Structural Diversity of Chitosan and Its Complexes. *Carbohydr. Polym.* **2000**, *41*, 237–247. [CrossRef]

56. Leceta, I.; Guerrero, P.; de la Caba, K. Functional Properties of Chitosan-Based Films. *Carbohydr. Polym.* **2013**, *93*, 339–346. [CrossRef]
57. Cervera, M.F.; Karjalainen, M.; Airaksinen, S.; Rantanen, J.; Krogars, K.; Heinämäki, J.; Colarte, A.I.; Yliruusi, J. Physical Stability and Moisture Sorption of Aqueous Chitosan–Amylose Starch Films Plasticized with Polyols. *Eur. J. Pharm. Biopharm.* **2004**, *58*, 69–76. [CrossRef]
58. Epure, V.; Griffon, M.; Pollet, E.; Avérous, L. Structure and Properties of Glycerol-Plasticized Chitosan Obtained by Mechanical Kneading. *Carbohydr. Polym.* **2011**, *83*, 947–952. [CrossRef]
59. Karabagias, V.K.; Giannakas, A.E.; Andritsos, N.D.; Leontiou, A.A.; Moschovas, D.; Karydis-Messinis, A.; Avgeropoulos, A.; Zafeiropoulos, N.E.; Proestos, C.; Salmas, C.E. Shelf Life of Minced Pork in Vacuum-Adsorbed Carvacrol@Natural Zeolite Nanohybrids and Poly-Lactic Acid/Triethyl Citrate/Carvacrol@Natural Zeolite Self-Healable Active Packaging Films. *Antioxidants* **2024**, *13*, 776. [CrossRef] [PubMed]
60. Štumpf, S.; Hostnik, G.; Primožič, M.; Leitgeb, M.; Salminen, J.-P.; Bren, U. The Effect of Growth Medium Strength on Minimum Inhibitory Concentrations of Tannins and Tannin Extracts against *E. coli*. *Molecules* **2020**, *25*, 2947. [CrossRef] [PubMed]
61. Schulz, H.; Özkan, G.; Baranska, M.; Krüger, H.; Özcan, M. Characterisation of Essential Oil Plants from Turkey by IR and Raman Spectroscopy. *Vib. Spectrosc.* **2005**, *39*, 249–256. [CrossRef]
62. Higueras, L.; López-Carballo, G.; Hernández-Muñoz, P.; Catalá, R.; Gavara, R. Antimicrobial Packaging of Chicken Fillets Based on the Release of Carvacrol from Chitosan/Cyclodextrin Films. *Int. J. Food Microbiol.* **2014**, *188*, 53–59. [CrossRef]
63. Priolo, M.A.; Gamboa, D.; Holder, K.M.; Grunlan, J.C. Super Gas Barrier of Transparent Polymer–Clay Multilayer Ultrathin Films. *Nano Lett.* **2010**, *10*, 4970–4974. [CrossRef]
64. Duan, C.; Meng, X.; Meng, J.; Khan, M.I.H.; Dai, L.; Khan, A.; An, X.; Zhang, J.; Huq, T.; Ni, Y. Chitosan as A Preservative for Fruits and Vegetables: A Review on Chemistry and Antimicrobial Properties. *J. Bioresour. Bioprod.* **2019**, *4*, 11–21. [CrossRef]
65. Friedman, M. Chemistry and Multibeneficial Bioactivities of Carvacrol (4-Isopropyl-2-Methylphenol), a Component of Essential Oils Produced by Aromatic Plants and Spices. *J. Agric. Food Chem.* **2014**, *62*, 7652–7670. [CrossRef]
66. Qu, B.; Luo, Y. A Review on the Preparation and Characterization of Chitosan-Clay Nanocomposite Films and Coatings for Food Packaging Applications. *Carbohydr. Polym. Technol. Appl.* **2021**, *2*, 100102. [CrossRef]
67. Brahmi, M.; Moumnassi, S.; Essifi, K.; Dumas, E.; Asehraou, A.; Tahani, A.; Gharsallaoui, A. Carvacrol-Loaded Montmorillonite–Caseinate Hybrids as Active Additives for the Development of Antimicrobial Alginate-Chitosan Microcapsules. *Appl. Clay Sci.* **2025**, *278*, 107996. [CrossRef]
68. Pajnik, J.; Dikić, J.; Milovanovic, S.; Milosevic, M.; Jevtic, S.; Lukić, I. Zeolite/Chitosan/Gelatin Films: Preparation, Supercritical CO_2 Processing, Characterization, and Bioactivity. *Macromol. Mater. Eng.* **2022**, *307*, 2200009. [CrossRef]
69. Sadeghnejad, A.; Aroujalian, A.; Raisi, A.; Fazel, S. Antibacterial Nano Silver Coating on the Surface of Polyethylene Films Using Corona Discharge. *Surf. Coat. Technol.* **2014**, *245*, 1–8. [CrossRef]
70. Nikulina, E.O.; Ivanova, G.V.; Kolman, O.I.; Ivanova, A.N.; Perestoronin, D.Y. Research of the Influence of Vacuum Packaging on the Quality and Safety of Meat Semi-Finished Products. *IOP Conf. Ser. Earth Environ. Sci.* **2021**, *677*, 032066. [CrossRef]
71. Hernández-García, E.; Vargas, M.; Torres-Giner, S. Quality and Shelf-Life Stability of Pork Meat Fillets Packaged in Multilayer Polylactide Films. *Foods* **2022**, *11*, 426. [CrossRef] [PubMed]

Disclaimer/Publisher's Note: The statements, opinions and data contained in all publications are solely those of the individual author(s) and contributor(s) and not of MDPI and/or the editor(s). MDPI and/or the editor(s) disclaim responsibility for any injury to people or property resulting from any ideas, methods, instructions or products referred to in the content.